Bachelor Thesis

DEVELOPMENT OF A PITCHING CONTROL FOR A FLAPPING WING MAV

Author:
Christian Chazo Paz

Director:
Óscar Flores Arias

July 2016

Acknowledgements

First of all, I would like to thank Óscar and Manolo for the opportunity to take part of this project, as well as for him continuous support and encouragement. I would also like to thank Gonzalo for showing me how to deal with his program and always being willing to help.

My friends deserve some kind of mention for somehow finding the energy to deal with me. Thanks for every laugh, every smile, and every *cri*.

And the biggest thank of all goes to my family. Their permanent help and support makes possible everything else.

Contents

List of Figures

List of Tables

Chapter 1

Introduction

1.1 Motivation

Humans have been able to fly for something more than a century. Aircraft technology has evolved extensively, but has been limited to fixed and rotatory wings. We still know very little when it comes to flapping wing flight, which means that we struggle when trying to fly at low speeds. Scaling laws with respect to a vehicle′s size play against small fixed wing vehicles [1][2]. Furthermore, low Reynolds aerodynamics are favourable to flapping mechanisms whilst fixed-wing aircraft suffer from low Reynolds effects. So many disadvantages make fixed wing vehicles unsuitable to operate at low speeds. Rotatory wings, where the airfoil speed is not directly dependant on the vehicle speed, offer the possibility of hovering as well as flying forwards which is a significant improvement with respect to fixed wings.

However, nothing can match the performance that nature has exhibited by means of birds, bats and insects. Various species of birds are able to fly at speeds over 120 body lengths per seconds, which is impressive when compared to a common airliner flying at 4 to 6 body lengths per second during cruise, or the fastest manned aircraft to be crafted (SR-71 'Blackbird') with no more that 32 body lengths per second [3]. Their turning performance is equally outstanding. A simple fruit fly can make a 90^o turn in 50 ms, which implies a yaw rate of 1800^o/s [4]. Roll rates achieved by a Barn Swallow can be as high as $5000^o/s$, an order of magnitude above what an acrobatic aircraft could achieve [3].

There are plenty potential applications that encourage developing flapping-wing vehicles. The small size, combined with very high maneuverability potential, makes MAV equipped with flapping wings suitable to reconnaissance and surveillance mis-

sions in hazardous or hardly accessible environments. On the other hand, the similarity to birds is an asset by itself; falconry is used to scare birds away from airport runaways, task that could be accomplished with falcon-like ornithopters[1] in a cheaper and more reliable way. Those are just a couple of examples of the uncountable applications that a technology with unmatched characteristics will imply.

1.2 The challenge ahead

Top performance comes with increased complexity. Bird and insect wings are flexible and articulated, and each species has several flapping patterns depending on the manoeuvre that the animal is trying to perform. On top of that, the low Reynolds aerodynamics offer different and unexplored mechanisms that make possible the flight of smallest insects. The understanding of these flapping wing flow phenomena is based primarily on observation. The first slow-motion film of an insect flying dates back to 1868 [5], but observations suitable for an aerodynamic analysis were only possible during the second half of the last century [6] [7].

Analysing the aerodynamics and dynamics of the small insects is already difficult, but trying to mimic is extremely challenging. Both thrust and lift have to be produced by the same moving surface and change greatly as the stroke goes on. That makes very difficult to attain stable flight. The straight level flight that airliners perform smoothly becomes a complicated task, and lateral manoeuvring would be even more challenging.

Other characteristics that add complexity to this technology is the natural flexibility that insects and birds posses. This includes the body as well as the wings and tail. Another issue is the variable inertia properties and forces on the whole body when considering the movable parts. Wing mass can reach up to 25% of the mass of even small bats and birds [3], that combined with wide flapping amplitudes result in significant inertia properties variation and inertial forces.

1.3 Working examples

In spite of the difficulties, several projects have already been developed and successfully flown. Grauer′s ornithopter [8] is able to maintain straight level flight for a couble of meters. This vehicles takes into consideration the inertia of the different movable surfaces as shown in Fig 1.1. This vehicle is too big to be considered a MAV,

[1] Aircraft based on flapping wings

but its flapping wing performance is remarkable. The pitch oscillations while free flying are as small as 3^o. However, the longitudinal flight presented on [8] exhibits some horizontal acceleration and pitch angle net gain after 3 flapping cycles of about 3^o. Taking into account the inherent complexities of trying to stabilize a body with movable parts and highly unsteady aerodynamic forces, their result is satisfactorily close to horizontal flight.

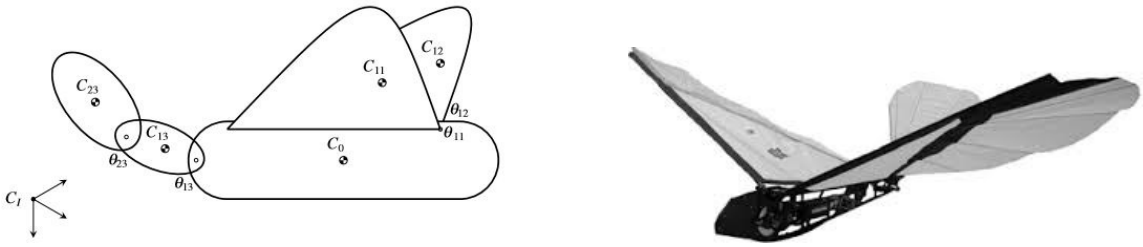

(a) Grauer's ornithopter multibody model (b) Vehicle picture

Figure 1.1: Vehicle developed at the University of Maryland [8]

The DelFly family is a group of MAVs developed by the University of Delft. In spite of their reduced size(DelFy Micro weights 3.07 grams [9] and DelFly Explorer, 20 grams [10]), they carry a camera onboard. The explorer used is to avoid obstacles as well as a barometer to control height Fig 1.2

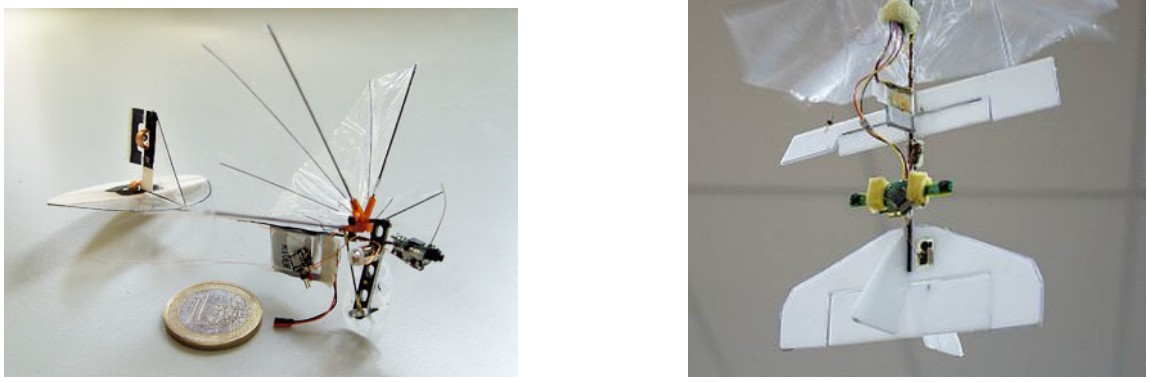

(a) DelFly Micro (b) DelFly Explorer

Figure 1.2: Project from the MAV Lab of the University of Delft [10][9]

1.4 Socioeconomic environment

Just as the Internet technology in the early nineties gave rise to many different applications, RPAS (Remotely Piloted Aircraft Systems) technologies should lead in the coming years to the development of a wide variety of different services. With those words, the European Commission describes the relevance of the civil use of remotely piloted aircraft systems [11]. Their operation as substitution of manned aviation results in economic savings, environmental benefits and reduced risk to human life.

The most immediate applications are those related to infrastructure and area monitoring. Unmanned vehicles allow operation in hazardous or hardly accessible environments. Specially when the vehicle mission is related to observation, obtaining an stable attitude is key in order to allow them to perform their task.

From 2001 to 2013, forest fires affected 116769 hectares each year only in Spain. Forest surveillance by means of UAV equipped with infrared cameras would allow earlier action and reduce the impact of such events. Other environmentally critical mission that is considered is the monitoring of emissions from burning coal [12].

In particular, flapping-wing technology is intended to be used in vehicles operated in low Reynolds. This means small vehicles flying slowly. Fixed-wing vehicles performance reduces significantly on that kind of flight, while flapping-wing get the most out of it. This would make them suitable for indoor surveillance, task that nowadays is executed by wall-mounted cameras or human guards, with their associated disadvantages such as reduced mobility or guard salary.

On top of that, the evolution of this kind of vehicles would be a key tool for transport of goods with high economic value per weight or when time is critical, such as the transport of organs to be transplanted. In a less immediate scenario, missions where physical interaction with the environment is required such as maintenance operations in hazardous environments or hardly accessible locations would make great use of the hovering capabilities of flapping-wing vehicles. Just like a hummingbird facing a flower.

1.5 Legal framework

The main issue about the legality of Unmanned Air Vehicles is that there is no clear regulatory framework in the European Union. This is holding back an industry with vast potential, since companies cannot design and develop commercial products if they still don't know what is going to be allowed by the final regulation.

The European Commission proposals concerning this vehicles follow the Riga Declaration on remotely piloted aircraft, "Framing the future of aviation", which states guidelines for the regulation of drones [13]. The following principles are stated:

- Drones need to be treated as new types of aircraft with proportionate rules based on the risk of each operation.
- EU rules for the safe provision of drone services need to be developed now.
- Technologies and standards need to be developed for the full integration of drones in the European airspace.
- Public acceptance is key to the growth of drone services.
- The operator of a drone is responsible for its use.

The actual implementation of this conditions on the legal framework will determine the impact that MAVs may have in our lives.

Chapter 2

Objectives and methodology

The main purpose of this project is to develop a pitching control for MAVs with flapping wings. This is one of the first issues that needs to be assessed in the flapping wing technology due to the unsteadiness of the aerodynamic forces. In order to achieve this goal, we define the specific objectives defined in 2.1, 2.2 and 2.3. A brief description of the available methods and tools is presented in 2.4.

2.1 Vehicle definition

The first stage of the problem is the definition of the vehicle. In order to analyse the pitch stability, a completely defined vehicle model has to be developed as a basis for the stabilization work.

Design problems are open since there are plenty of design parameters that have to be decided rather than obtained with equations. The overall geometry will be a slender body with two wings and the stabilisation mechanism at the rear end of the body. Later, the variables that have a direct influence on the dynamic and aerodynamic performance will be adjusted to fulfil the level flight condition. The main reference to obtain realistic relations between the different parameters will be birds. Plenty of correlations are present on the literature and provide a good estimation of the main variables, such as the relation between the mass and the cruise speed[3][14]. *AeroFlaps* will be used in this stage of the project to estimate the viability of each combination of parameters of the defined parametric study.

2.2 Straight level flight

Once the vehicle is defined, it will be tested in *DyMoFlpas*. The objective is to be able to maintain level flight. The vehicle obtained with *AeroFlaps* will need modifications to be able to sustain flight as the aerodynamic forces now depend on the evolution of the dynamics of the MAV. A simple tail device will be required in any case since the wings themselves are not likely to be stable.

2.3 Pitch damping

The vehicle will oscillate on the symmetry plane due to the unsteady aerodynamic forces. The frequency of these oscillations will be that of the flapping motion of the wings, and the amplitude will depend on the efficiency of the method used to damp the motion. In principle, we will evaluate two different mechanisms for stabilisation:

Aerodynamic tails As used in conventional fixed wing aircraft offer the possibility of adding a restoring moment. Both fixed and mobile tails are options to be considered.

Inertial control Following the example of some birds and insects, an articulated body can be used to counteract the aerodynamic moment produced by the wings. However, an articulated fuselage is not a convenient characteristic for an aircraft due to the manufacturing complexity and payload management issues. However, placing a relatively small mass on the rear end of the vehicle could be enough.

2.4 Methods and tools

AeroFlaps [15] is a potential aerodynamic solver that consists of a unsteady 2D panel method based on [16] that yields the forces acting on two wings with given motion. This low-order model is based on a potential approximation that neglects viscous effects. This is a strong approximation taking into account the moderate Reynolds number of flapping wings. However, the purpose of this project is to analyse and compare the performance of preliminary pitch control mechanisms, in a fast and efficient way. Higher order models that solve the complete Navier-Stokes equations are costly and highly time consuming, not suitable for this kind of analysis. High-order simulations, that take into account the viscous effects that potential methods neglect, are the next step after the best control option is determined.

DyMoFlaps [17] (**Dy**namic **Mo**del for **Flap**ping wings) is a model of the longitudinal and symmetric flight of a MAV. An earlier version of *AeroFlaps* is integrated into it to compute the aerodynamic forces taking into account the dynamics of the vehicle; the new version will be implemented in the present project to better estimate the forces produced by the wings flapping. In *DyMoFlaps*, the orientation of the vehicle is described using quaternions[18], to avoid the singularities present on the regular Euler angle rotations. A second order Adam Bashforth numerical scheme is used to compute the motion of the body. Since this method requires information of the previous time steps, an Euler method is used to perform the first time step of the simulation.

Chapter 3

Vehicle definition

There are some requirements that every aerial vehicle needs to fulfil. A vehicle must produce lift enough to counteract its weight and thrust enough to overcome its drag. Furthermore, it needs to be able to maintain its orientation as desired so that the flight is controllable or, at least, predictable. The later is the ultimate goal of this project, and the one that will receive more attention, but first thrust and lift need to be dealt with to allow flight.

In fixed-wing aircraft thrust and lift are generated by different aircraft elements. This is not the case for flapping-wing aircraft, since both tasks belong to the wings. Therefore, the generation of those forces is highly coupled. Furthermore, those forces are changing greatly across the flapping cycle, even with sign changes that result in instantaneous vertical forces pushing the body down during the up-stoke. This makes the task of obtaining a smooth trajectory with fixed orientation more complicated than for convenvional fixed-wing aircraft. Another difficulty to achieve a smooth trajectory is the inertial forces due to the wing strokes. The mass of the wing is a significant portion of the weight of some birds and big insects. For example, an osprey can have as much as 28%[3] of its body weight on the wings. Those forces, however, will not be considered during the development of this project. Since the centre of mass of the body sill be reasonably close to the centre of mass of the wings, the moment caused by the inertia will be small when compared to the aerodynamic moment of the wing and the moment created on the tail device.

3.1 Design process structure

The first step on the design is to define the overall geometry of the vehicle. It will be described in terms of nondimensional parameters that will scale with the final chord of the vehicle.

After that, the level flight condition is analysed to decide the design mass and cruise speed. Similarly, the horizontal balance between drag and thrust will be analysed.

The wing kinematics are studied next. The wing motion is composed of several rotations that depend on several parameters. The target at this point is to define the criteria to reduce that set of parameters to an smaller one for the parametric study that is performed after the whole geometry and motion is defined.

On the parametric study, a range of values is given to the free parameters and the results are valued based on the criterion given. With the selected set of parameters, as well as the corresponding chord size, final values for the vehicle geometric and kinematic variables are obtained.

3.2 First geometric considerations

The overall geometry of the vehicle is described next. The vehicle will be composed of a body, two rectangular wings and a tail device connected by a rigid element to the main body. Both manufacturing convenience and nature flappers have been taken into account in the design. The tail devices are thoroughly discussed in chapter 4.

3.2.1 Wings

The wings do not have any sweep angle or geometric twist. That kind of performance refinement mechanisms are an option to be considered when designing a MAV, but they do not play a main role when identifying which tail device will work better. Therefore rectangular, flat wings will be used. The wings are defined with parameters that are non-dimensional with the chord, since the chord value will be determined to match the surface required for maintaining flight.

The centre of rotation of the wing, or flapping centre, will be on the plane of symmetry of the vehicle, at the position in the middle of the leading edges of the wings. The inter-wing distance will be assigned a value equal to the chord. This leaves sufficient space for a body with the flapping mechanism in between.

$$\alpha_d = \frac{d}{c} = 1 \tag{3.1}$$

where d is the distance between the wings and α_d the corresponding nondimensional parameter (not to be confused with the angle of attack of the wing, α).

In this document, the variable b will correspond to the span of each of the individual wing rather than the usual total span. Being AR_w and AR_v the aspect ratio of one of the wings and the aspect ratio of the vehicle, respectively:

$$b = AR_w c \tag{3.2}$$

And the total span will be

$$span = 2b + d = (2AR_w + \alpha_d)c \tag{3.3}$$

The total aspect ratio of the vehicle can be computed as a function of the other parameters:

$$AR_v = \frac{span^2}{S_{wings}} = \frac{((2AR_w + \alpha_d)c)^2}{2c^2 AR_w} = \frac{(2AR_w + \alpha_d)^2}{2AR_w} \tag{3.4}$$

Common values for the aspect ratio in small flappers that may serve as inspiration for a MAV can be found in [3]. Values range mainly from $AR = 4$ to $AR = 7$. The ornithopter developed in [8] posses an aspect ratio $AR = 4.4$. It was decided that aspect ratio for each wing shall be $AR_w = 2$. It makes a total span of the vehicle equal to 5 chords, and a total aspect ratio of $AR_v = 6.25$.

3.2.2 Body

The fuselage shape will be cylindrical. The front and rear end of the cylinder will be streamlined to obtain smooth flow and avoid detachment. The idea is to avoid detachment so that the drag is reduced as much as possible. A regular cylinder with no aerodynamic shaping has a drag coefficient of roughly unity over a large range of Reynolds number (taking the cross-section area as reference). That drag coefficient is significantly bigger than the expected from the streamlined body, since the detachment on the sharp edges is avoided.

From the rear end of the body emerges a rigid element that will connect with the tail device. Such rigid element shall be light and smooth to avoid affecting the performance. Its proposed length will be determined during the design of the tail device.

The body mass properties will be described in section 3.7 after the preliminary aerodynamic performance of the vehicle has been computed.

All the mass of the vehicle is on the body, where payload, batteries, servos, sensor and control unit are expected to be.

3.3 Level flight condition

3.3.1 Reference frames

Three reference frames are used by the codes, being the three of them orthogonal and right-handed. The first of the is the inertial reference frame, formed by the axis X,Y and Z fixed at point I, so the coordinate system is $IXYZ$. The X axis points towards the rear end of the vehicle and the Z axis points upwards. The body fixed reference frame is designated as $Ox_By_Bz_B$. Since in this project the motion is confined to a vertical plane, the body fixed reference frame orientation is obtained by performing a rotation around the Y axis. This rotation represents the pitch of the vehicle, θ, the motion that this project aims to damp. During the *AeroFlaps* simulations used for the parametric study, this rotation does not take place since the vehicle body is clamped in front of the free stream. The inertial and body fixed reference frames are displayed on Fig. 3.1a.

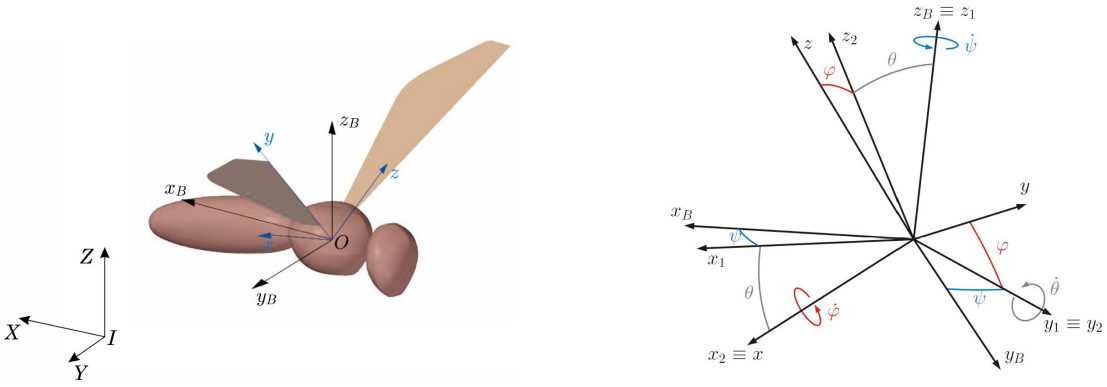

(a) Inertial and body fixed reference frames

(b) Body fixed and wing reference frames

Figure 3.1: Reference frames used by the codes

The position of the wing relative to the body is defined with the angles.

- Sweep angle ψ

- Pitch angle θ_w
- Flapping angle φ

The wing reference frames remain attached to the wings, with the y axis coincident with the leading edge and the origin coincident with the that of the body reference frame. Each wing has its own reference frame and they must be handled separately. Their rotations to go from $Ox_By_Bz_B$ to $Oxyz$ as shown in Fig. 3.1b are defined with the same sign criteria, but since the motion has to be symmetric, the sign of the flapping and sweep angles must be the opposite, thus making necessary the differentiation between right wing and left wing reference frames. The rotations are performed in the following order. First, a rotation ψ around z_b to obtain $x_1y_1z_1$. Then, a rotation θ_w around the axis y_1 to obtain $x_2y_2z_2$. Finally, the rotation φ around the x_2 axis is used to obtain xyz, the wing axes.

3.3.2 Vertical force balance

The mass and speed of the vehicle are directly related by the equilibrium of vertical forces.

$$\frac{1}{2}\rho U_\infty^2 S\overline{C}_L = W \rightarrow \frac{1}{2}\rho U_\infty^2 \overline{C}_L = \frac{W}{S}, \tag{3.5}$$

where $\frac{W}{S}$ is defined as wing loading and $\overline{C}_L$ is the period average lift coefficient:

$$\overline{C}_L = \frac{1}{\frac{1}{2}\rho U_\infty^2 S_w}\frac{1}{T}\int_0^T F_z(t)\mathrm{d}t \tag{3.6}$$

where $S_w = c^2 AR_w$ is the surface of one of the wings and F_z the vertical force component, expressed in body axes. As the equation shows, the smaller the speed, the lower the possible wing loading. Here is where scaling laws punish small vehicles: a relatively larger surface is required to withstand their weight due to the small speed at which they fly.

Note that the force coefficients refer to the forces acting on the vehicle, therefore including the force contribution from both wings, although the reference surface refers to one of the wings.

3.3.3 Low Reynolds effects

Low Reynolds effects play in favour of the small flapping wings. In particular, the effect known as dynamic stall allows for a higher lift coefficient that quasi-steady

values[19]. This effect consist on the formation of leading-edge vortex on the upper surface of the wing at high angles of attack, that remains attached during the stroke. In 2D flows, this vortex builds up its strength until it detaches and a vortex of opposite sign is formed on the trailing edge. That pattern repeats , leaving a trail of vortex of alternating sign known as Kármán vortex street. However, when 3D effects are present, the leading edge vortex detachment is delayed, so it remains attached long enough to assist during the whole stroke [20].

3.3.4 Wing loading, mass and cruise speed

Low Reynolds effects will increase the average lift coefficient during the flapping cycles, but not beyond the order of unity. Therefore, a significant decrease of the wing loading is unavoidable for slower vehicles. Fig 3.2 shows the relation between the mass and the flying speed of a representative sample of natural flappers. In general, the mass of a vehicle is something that has to be decided, rather than computed from other variables, since it is highly related to the purpose or kind of mission intended for the vehicle. Since the purpose is MAVs, a mass of 100 grams is selected as design point, with a target speed of 10 meters per second in accordance with Fig. 3.2. The final speed on the simulation may be slightly different since the resulting speed will result from the balance between the actual thrust and the drag.

Relations between wing loading and weight for several animals and aircraft are shown in Fig. 3.3. Values for the wing loading expected for the selected mass of 0.1kg range between 20 and 50 N/m^2. After surface of the wing is selected, the wing loading will be computed and checked against this reference values.

3.4 Thrust and drag balance

As Eq. 3.5 determined the vertical balance of forces that guaranteed that the vehicle shall not climb or descend, a similar equilibrium equation between thrust and drag is necessary to achieve constant speed forward flight,

$$T = D \Rightarrow \frac{1}{2}\rho U_\infty^2 S_w \overline{C}_T = \frac{1}{2}\rho U_\infty^2 S_f C_D \Rightarrow \overline{C}_T = \frac{S_f}{S_w} C_D \tag{3.7}$$

where $S_f = \pi \frac{d^2}{4}$ is the frontal surface of the fuselage and C_D its drag coefficient with the frontal surface of the cylinder as reference surface. The coefficient of thrust, $\overline{C}_T$, can be obtained by integrating the force $-F_x(t)$ in body axes in a way analogous

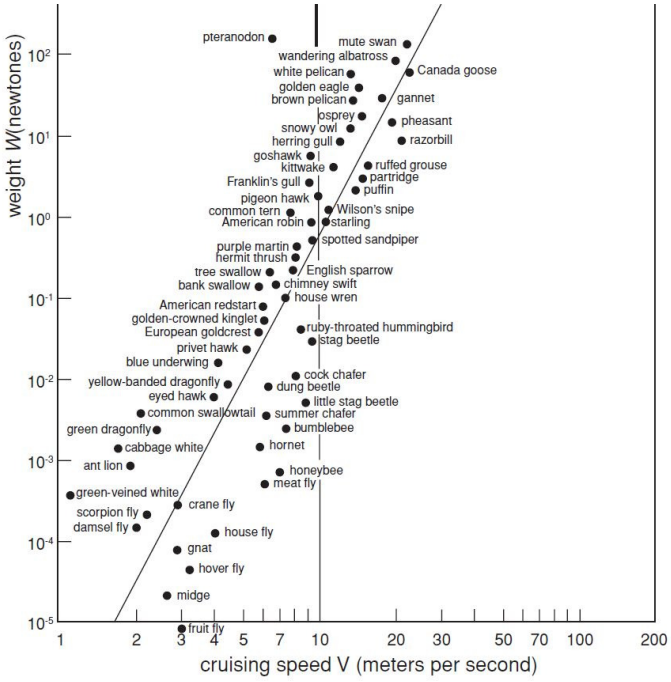

Figure 3.2: Correlation between weight and cruise speed[3]

to equation (3.6). The negative sign is added because the x-axis points towards the rear end of the vehicle, and the thrust is defined as force forward.

The final values of the surfaces are still to be defined, but the ratio between them can be obtained, assuming that the diameter of the fuselage equals the distance between the wings, $d = c$:

$$\frac{S_f}{S_w} = \frac{\pi(\frac{d}{2})^2}{cb} = \frac{\pi(\frac{\cancel{c^2}}{4})}{\cancel{c^2}AR} = \frac{\pi}{4AR} = \frac{\pi}{8} \tag{3.8}$$

A threshold value for the thrust coefficient must be established to assess the validity of the simulation results of the parametric study that will be performed. A value of the drag coefficient of the body is necessary for that in accordance with equation 3.7. A conservative estimation is $C_D = 1$. It was discussed earlier that this value would correspond to a cylinder that has not been streamlined. Therefore, the nominal condition for the thrust coefficient is:

$$\overline{C}_T \geq \frac{\pi}{8} \tag{3.9}$$

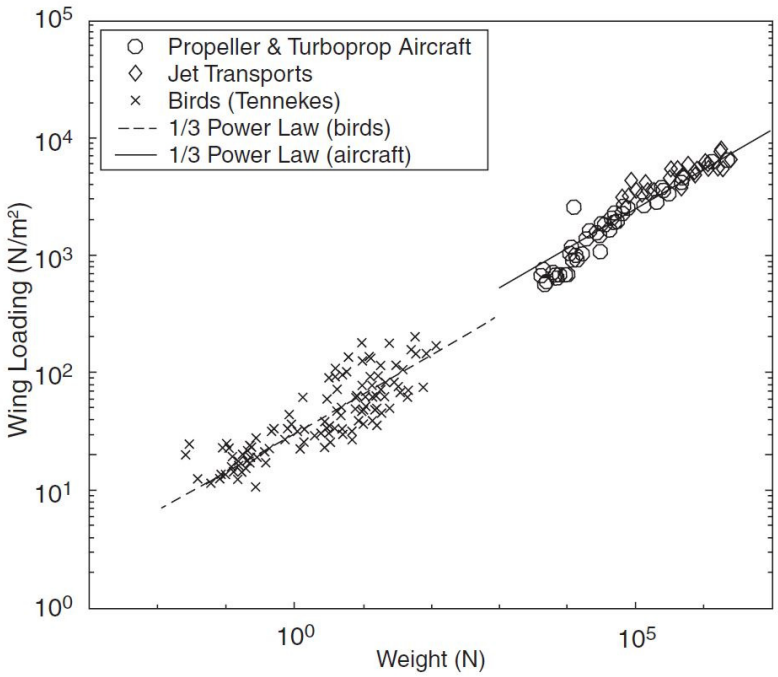

Figure 3.3: Wing loading vs animal weight[3]

3.5 Wing kinematics

3.5.1 Wing motion laws

Pitch and flapping angles will evolve with time, while the sweep angle remains equal to zero. Pitch has a strong influence on the vertical force since it determines the angle of attack of the wing. On the other hand, the flapping motion determines the amount of thrust generated, since the change of incident speed direction tilts the force forward during both the up-stroke and the down-stroke. Working with those two effects is possible to fulfil the equilibrium of forces, and adding sweep motion to the wing would only couple the vertical and horizontal forces, making harder to determine the best configuration (asides from adding a variable to the parametric study and therefore increasing drastically the computational cost of the problem) The motion is determined by the following functions:

$$\theta_w(t) = \theta_m + \theta_0 \sin(\omega t + \phi) \tag{3.10}$$

$$\varphi(t) = \varphi_m + \varphi_0 \sin(\omega t) \tag{3.11}$$

where ϕ is the phase delay between both rotations and ω is the angular frequency of the of the motion. Those variables will be defined later.

Flapping motion

The output from *AeroFlaps* consist on the normal and tangential components of the force on the wing, given in terms of the force coefficients C_n and C_t, respectively. Those instantaneous forces in wing reference frames need to be converted into body axes by rotating the force with the angles described above.

$$\begin{bmatrix} -C_T \\ 0 \\ C_L \end{bmatrix}_b = R_\psi^T R_\theta^T R_\varphi^T \begin{bmatrix} C_t \\ 0 \\ C_n \end{bmatrix}_w \tag{3.12}$$

For the simplified case with $\psi = 0$, and taking into consideration that the lateral force will remain zero due to symmetry:

$$-C_T = C_t \cos\theta_w + C_n \sin\theta_w \cos\varphi \tag{3.13}$$

$$C_L = -C_t \sin\theta_w + C_n \cos\varphi \cos\theta_w \tag{3.14}$$

The force transmitted to the vehicle is reduced with the flapping angle. Therefore, to minimise this penalty the mean flapping angle φ_m is set to zero.

The value for φ_0 and the wing tip vertical displacement are directly related:

$$h_{t,max} = R_f \sin\varphi_0 = \alpha_t c \tag{3.15}$$

where R_f is the flapping radius at the tip and α_t is the maximum wing tip vertical displacement, in chords. The flapping centre will be located at the origin of the body and wing reference frames, so the flapping radius will be the distance from the origin to the wing tip.

$$R_f = \frac{d}{2} + b = c\left(\frac{\alpha_d}{2} + AR_w\right) = c\left(\frac{1}{2} + AR_w\right) \tag{3.16}$$

where α_t is the maximum wing tip vertical displacement, in chords.

By plugging the formula for R_f on equation (3.15), the value of the flapping angle amplitude is defined as a function of the non-dimensional parameters of the problem, which is essential since the chord (and therefore any other dimensional quantity) will not be determined until after the parametric study.

$$R_f \sin\varphi_0 = \alpha_t c \Rightarrow \cancel{\left(\frac{\alpha_d}{2} + AR\right)} \sin\varphi_0 = \alpha_t \cancel{\left(\frac{\alpha_d}{2} + AR\right)} \Rightarrow \varphi_0 = \sin^{-1}\left(\frac{\alpha_t}{\frac{\alpha_d}{2} + AR}\right) \tag{3.17}$$

By changing the value of α_t, the thrust obtained is modulated. On the other hand, $\theta_w(t)$ has to be adjusted to generate lift enough.

Pitching motion

During the up-stroke, the chord of the should align with the incident flow to reduce the negative vertical force created. During the down-stroke, is should produce an acceptable value for the angle of attack of the wing. The following equations are defined for the both instants of the cycle where $\varphi(t) = 0$, the instants of maximum wing vertical speed.

$$\theta_{w,up\_stroke} = \theta_{w,max} = \theta_m + \theta_0 \tag{3.18}$$

$$\theta_{w,down\_stroke} = \theta_{w,min} = \theta_m - \theta_0 \tag{3.19}$$

To obtain positive and negative peak values of θ_w when $\varphi = 0$, a phase delay $\phi = \pi/2$ is required. To determine the values of θ_m and θ_0, the actual angle of attack that the wing is going to see when it flaps and pitches should be obtained. The angle of attack will depend on the orientation of the wing and its velocity.

Let's define the vertical displacement and speed of any point along the leading edge of the right wing.

$$h(y,t) = h_{t,max} \sin(\omega t)\frac{y}{R_f} = \alpha_t c \sin(\omega t)\frac{y}{R_f} \tag{3.20}$$

$$\dot{h}(y,t) = h_{t,max}\omega \cos(\omega t)\frac{y}{R_f} = \alpha_t c\omega \cos(\omega t)\frac{y}{R_f} \tag{3.21}$$

Since the velocity depends on the span as expressed on equation (3.21), the angle of attack will vary along the span:

$$\Delta\alpha_{flap} = \arctan\left(\frac{\dot{h}(t,y)}{U_\infty}\right) \tag{3.22}$$

And the total angle of attack would be:

$$\alpha(t,y) = \theta_w(t) + \Delta\alpha_{flap} \tag{3.23}$$

The angle of attack will be higher on the tip and smaller towards the wing root. A point of the span has to be selected to represent the wing. In rotatory-wing aircraft analysis, where the velocity of the airfoil is proportional to the distance to the centre of rotation as in this case, the 75% span is usually used as if it represented the whole wing. Taking it as reference, the angle of attack due to flapping at point $y = 0.75R_f$ will be used as basis to estimate the suitable pitch mean value and amplitude. Plugging inside (3.22) the expression (3.21) evaluated at $y = 0.75R_f$:

$$\Delta\alpha_{flap} = \arctan\left(\frac{\alpha_t c\omega\cos(\omega t)}{U_\infty}0.75\right) \tag{3.24}$$

The expression for $\alpha(t)$, equation (3.23), is evaluated at the middle of the upstroke ($\cos(\omega t+\phi) = 1$) and the downstroke ($\cos(\omega t+\phi) = -1$). During the upstroke, a value of $\alpha = 0$ is assigned. During the downstroke, the value is left as a parameter since it will be swept on the parametric study.

$$\alpha_{up} = \theta_m + \theta_0 - \arctan\left(0.75\alpha_t\frac{c\omega}{U_\infty}\right) = 0 \tag{3.25a}$$

$$\alpha_{down} = \theta_m - \theta_0 + \arctan\left(0.75\alpha_t\frac{c\omega}{U_\infty}\right) \tag{3.25b}$$

By solving the system of equations (3.25) for θ_0 and θ_m:

$$\theta_m = \frac{\alpha_{down}}{2} \tag{3.26}$$

$$\theta_0 = \arctan\left(0.75\alpha_t\frac{c\omega}{U_\infty}\right) = \arctan\left(0.75\alpha_t k\right) - \theta_m \tag{3.27}$$

where $k = \frac{c\omega}{U_\infty}$ is the reduced frequency[1]. The reduced frequency measures unsteadiness by comparing the time that takes to flap the wing to the time required to cover one chord [3][21].

$$k = \frac{\omega}{\frac{U_\infty}{c}} = \frac{\frac{2\pi}{T}}{\frac{1}{t_{ch}}} \propto \frac{t_{ch}}{T} \tag{3.28}$$

where t_{ch} is the characteristic time which covers one chord and T the flapping period. A reference value for this parameter can be found in Fig. 3.4, where the reduced frequency is expressed as $\tilde{k} = \frac{c\omega}{2U_\infty}$. This figure gives an order of magnitude to have an idea about the range of values that will be used on the parametric study.

[1]This parameter is often defined in the literature as $\tilde{k} = \frac{c\omega}{2U_\infty}$

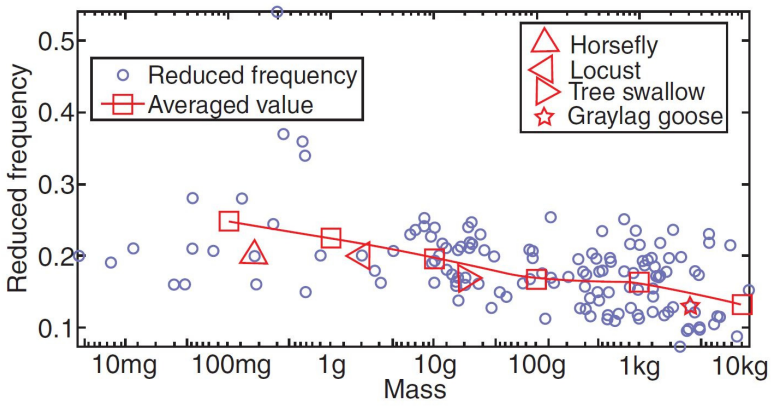

Figure 3.4: Correlation between weight and reduced frequency[3]

3.5.2 Wing kinematics summary

The resulting motion laws are:

$$\theta_w(t) = \theta_m + \left(\arctan\left(0.75\alpha_t k\right) - \theta_m\right)\sin\left(\omega t + \phi\right) \tag{3.29}$$

$$\varphi(t) = \sin^{-1}\left(\frac{\alpha_t}{\frac{\alpha_d}{2} + AR}\right)\sin\left(\omega t\right) \tag{3.30}$$

There are three parameters on equations (3.29) and (3.30) that have not been assigned a value.

Mean pitch angle (θ_m): The main influence of this parameter is on the vertical force, since the angle of attack during the downstroke is proportional to it.

Wing tip flap amplitude coefficient (α_t): The amplitude of the flap will be generating the thrust due to the change of the angle of incidence of the blade, that will tilt the resulting aerodynamic force forward.

Reduced frequency (k): This parameter will have an effect on both the thrust and the lift. Notice that on equations (3.29) and (3.30) ω is present. The code computes it using the reduced frequency, giving arbitrary values to c and U_∞ that have no influence on the resulting coefficients.

The rest of variables and design parameters have been already defined or depend on the three mentioned and the chord, as summarised in table 3.1

α_d [−]	1	AR_w [−]	2
$\frac{S_f}{S_w}$ [−]	$\frac{\pi}{8}$	AR_v [−]	6.25
R_f $[m]$	$2.5c$	f $[Hz]$	$2\pi k\frac{U_\infty}{c}$
θ_0 $[deg]$	$\arctan(0.75\alpha_t k) - \theta_m$	φ_0 $[deg]$	$\sin^{-1}\left(\frac{\alpha_t}{\frac{\alpha_d}{2}+AR}\right)$
ϕ $[deg]$	90	φ_m $[deg]$	0

Table 3.1: Values for the variables and parameters to be used in the simulation

3.6 Parametric study

The value of the coefficients $\overline{C}_L$ and $\overline{C}_T$ of the wings will be computed with *AeroFlaps*. The usage of *AeroFlaps* means that the speed is fixed and the pitch angle of the vehicle is zero. The coefficients will be computed for various values of the remaining parameters: θ_m, α_t and k. A range of values for the three parameters has to be defined.

- The mean pitch angle is half of the angle of attack that the 75% span will see according to equation (3.26). A reasonable limit to avoid stall issues, taking into account the dynamic stall explained on section 3.3.3, is 16^o. Therefore, the upper limit for the mean pitch angle is $\theta_m = 8^o$. The lower limit will be selected to be $\theta_m = 3^o$, and the increments will be of 1^o.
- The wing tip flap amplitude is expected to be of the order of one chord. The range of values was between $\alpha_t = 0.8$ and $\alpha_t = 1.2$ in increments of 0.1
- The reduced frequency will range from 0.55 to 0.8 in increments of 0.05. Although the literature showed in Fig. 3.4 that birds usually flap at smaller reduced frequencies, forces at reduced frequencies below the values presented were not sufficient.

3.6.1 Simulation details

AeroFlaps is used to perform the simulation with the range of parameters selected. This program requires several input parameters to perform the simulation.

- Chordwise and spanwise number of panels for the discretization of the wings. A higher number of panels would allow for a higher precision, but at an increased computational cost. The purpose of this project is to quickly draw

an estimation on the performance of the tail device before implementing it on a higher-order method code. Therefore, a large number of panels would not be beneficial for this project. The numbers of panels divisions selected are 4 (chordwise) and 9 (spanwise).

- The time step will be selected in accordance with the code developer [15][16].

$$dt = \frac{1}{4}\frac{i_{panels}c}{U_{ch}} \tag{3.31}$$

where i_{panels} is the number of chordwise panels and U_{ch} is the highest velocity that will see the wing, taking into account the flapping and pitching motion as well as the free stream velocity.

- The wake is modelled by shedding an array of panels from the trailing edge of the wing each time step. Those panels positions are stored and move freely with the flow, allowing wake roll-up. It is necessary to select a number of wake panels to be stored before the older ones (further away from to wings, and therefore with less influence on it) are deleted. Since the time simulated is two complete cycles, all the panels will be stored without significant computational time increase.

- The time simulated will be two complete flapping cycles. Since the motion is fully prescribed, the only difference between each cycle is the wake that has been stored. After one cycle, the wake shed is 7.75 chords long at the flapping frequency selected. The wake panels that are 5 chords downstream of the vehicle have negligible effect on the forces [15]. Therefore, the forces on the second period are computed with a wake that is long enough.

Panel resolution

The number of panels for the simulations was 4 (chordwise) and 9 (spanwise, including both wings). In order to check if this discretization gives a reasonable solution, a simulation with the final parameters selected was performed with a panel number of 8x17. In Fig. 3.5 the forces coefficients obtained on both simulations are plotted together. The results are similar with a maximum error of 4.5% of the force peak to peak amplitude, but the time consumed increases by an order of magnitude. The 4x9 panel division was kept since they slight precision increase does not pay off for the increased computational time.

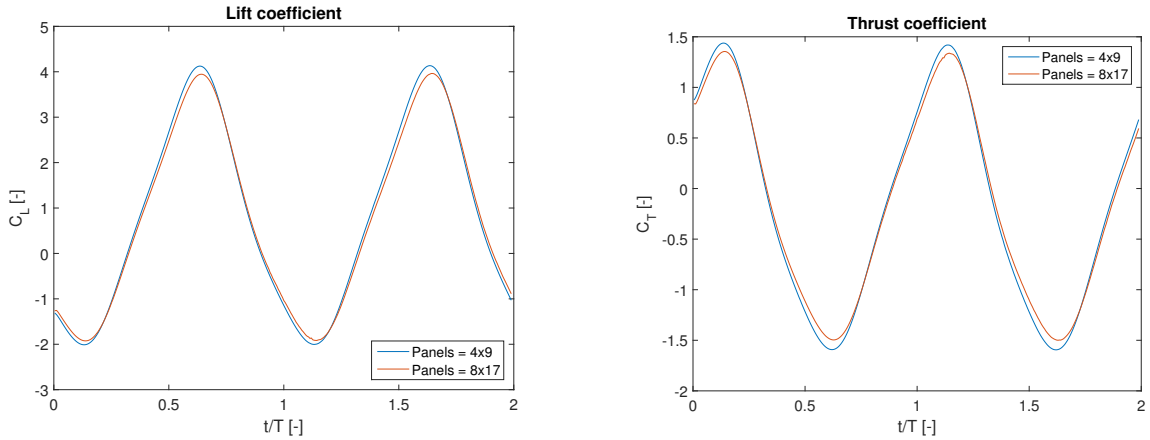

(a) Lift (b) Thrust

Figure 3.5: Forces under different panel resolutions

3.6.2 Results selection criteria

The first criterion is the minimum thrust required. In equation (3.9) the minimum thrust coefficient for a simulation to be acceptable was defined. Every simulation unable to fulfil it is discarded. On Fig. 3.6 and Fig. 3.7

For the remaining simulations, the required wing surface is computed. It is done by solving equation (3.5) for surface.

$$S = \frac{mg}{\frac{1}{2}\rho U_\infty^2 \overline{C}_L} \tag{3.32}$$

where the air density used was sea level standard ($\rho = 1.225$ kg/m^3) and the average lift coefficient is obtained from the simulation result.

After the surfaces have been obtained for the suitable simulations, the best has be selected. It was determined that the one with the smallest wing surface would be the best result, for several reasons:

- Smaller wing mass and therefore lower inertial forces while flapping. The reduced wing mass means that more payload mass is possible, since the total mass was fixed. Furthermore, a bigger wing would incur significant bending moment increase, which would require additional structural weight.

- The smaller inertial forces will also make our simulations more valid since the wing inertia is to be neglected. Neglecting bigger inertial loads would be more unrealistic than neglecting smaller ones.

- Since the aspect ratio is fixed, smaller wing surface means smaller chord. Smaller chord means that the whole vehicle is scaled down since the design lengths were adimensionalized with chord. A smaller vehicle is desired because it would also mean reduced structural weight, and because this project is motivated by the development of MAVs.

3.6.3 Final wing shape and motion

The resulting wing surface, corresponding to θ_m = 8^o, α_t = 1.1 and k = 0.8 is S_w = 0.0212 m^2. Two of the parameters, k and θ_m are maxed out. This is because those parameters allow a reduced wing surface to obtain the same averaged forces on a cycle. Its limitation comes from other design considerations, such as stall problems due to excessive local angle of attack or excessive flapping frequency. The feasibility of this result has to be checked, and for that reason all the resulting variables and parameters are summarised on table 3.2.

α_t $[-]$	1.1	θ_m $[deg]$	8
k $[-]$	0.8	S_w $[m^2]$	0.0212
C_T $[-]$	0.402	C_L $[-]$	0.7551
C_{My} $[-]$	-0.2724	α_d $[-]$	1
c $[m]$	0.1030	b $[m]$	0.2059
AR_w $[-]$	2	AR_v $[-]$	6.25
m $[kg]$	0.1	WL $[N/m^2]$	23.1245
R_f $[m]$	0.2575	f $[Hz]$	12.37
θ_0 $[deg]$	25.54	φ_0 $[deg]$	26.10
ϕ $[deg]$	90	φ_m $[deg]$	0

Table 3.2: Values for the variables and parameters of the resulting vehicle

When discussing the level flight equation (3.5), the wing loading of the vehicle was not determined since it depended on the surface. Now, the obtained value can be compared with the obtained. Fig. 3.3 showed the correlation between wing loading and weight. For a vehicle slightly below W = 1 N, a wing loading around $20 - 30$ N/m^2 was expected. The final vehicle has a wing loading of 23.1245 N/m^2 so the value is consistent with the nature correlation.

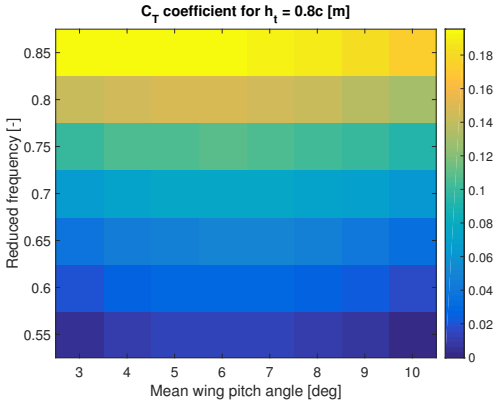

(a) $\alpha_t = 0.8$

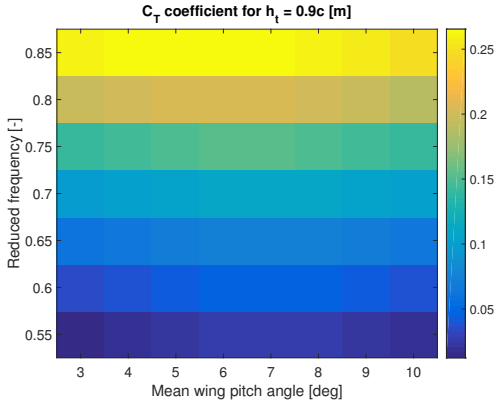

(b) $\alpha_t = 0.9$

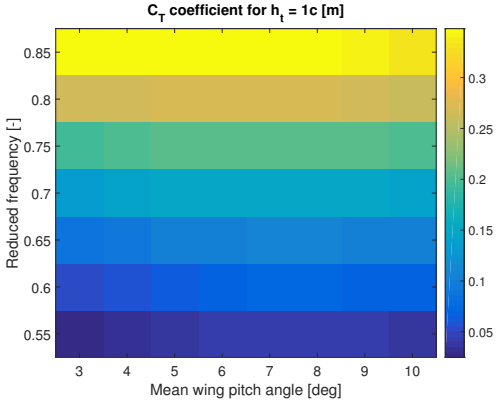

(c) $\alpha_t = 1.0$

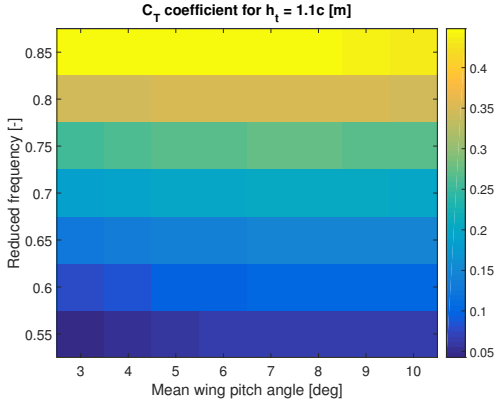

(d) $\alpha_t = 1.1$

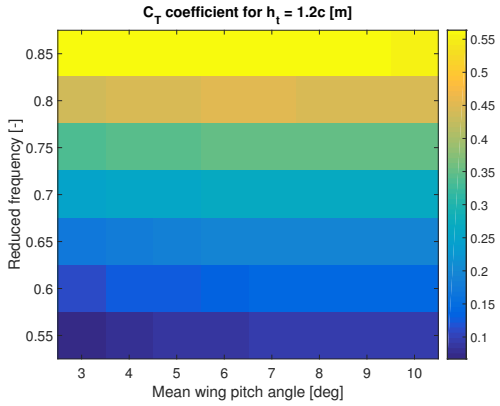

(e) $\alpha_t = 1.2$

Figure 3.6: Thrust coefficients

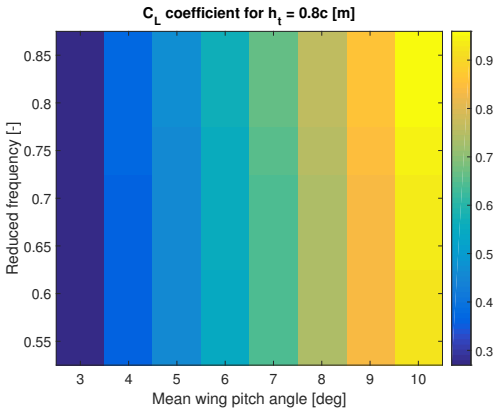

(a) α_t = 0.8

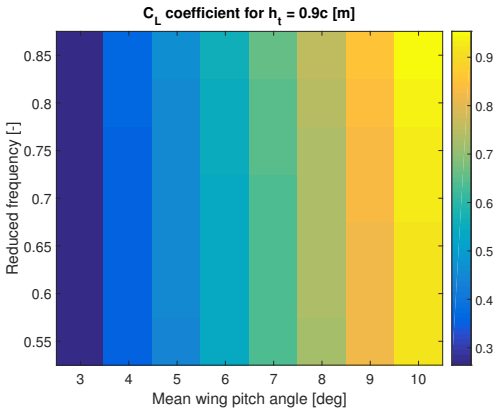

(b) α_t = 0.9

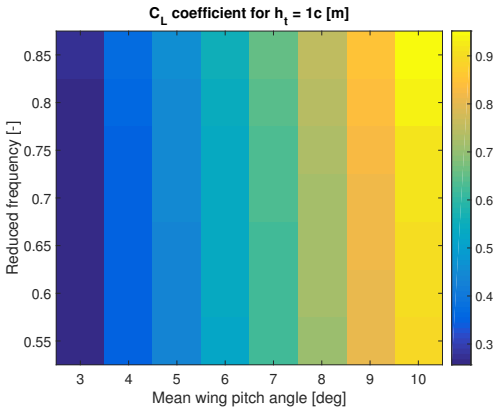

(c) α_t = 1.0

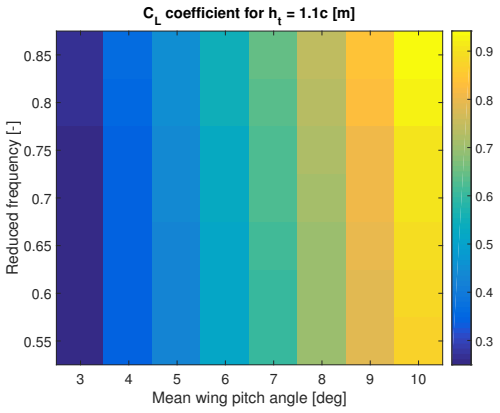

(d) α_t = 1.1

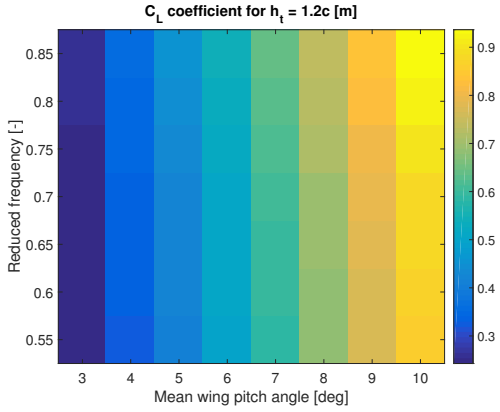

(e) α_t = 1.2

Figure 3.7: Vertical force coefficients

The flapping frequency is $f = 12.37\ Hz$. This frequency is higher than the average in nature. While this value is higher than the average for animal of similar size, common diving petrels with average mass similar to the one of this vehicle (133g) beat their wings with a frequency of 12.3 Hz [14], so this value is not out of the realistic.

3.7 Inertial properties and centre of mass

The mass distribution of the body is still to be determined. It will define the moment of inertia, which is necessary to compute the motion that the moments obtained in the simulation will produce.

The fuselage of the vehicle will be a streamlined cylinder with a diameter of one chord. The mass will be modelled as a smaller cylinder with plain ends. That cylinder will have a radius $r_c = 0.4c = 0.0412\ m$ and a length $L_c = c = 0.103\ m$. The radius is slightly smaller than the inter-wing distance to allow for some clearance. From an inertial standpoint, it would be better to have the mass distributed on a longer shape to increase the moment of inertia and thus reduce the angular accelerations. However, that would not be so convenient in terms of manufacturing. A cylinder of those dimensions with all the mass of the aircraft assigned to it, would have a density $\rho_c = 182.2\ kg/m^3$. Since batteries and motors will have a density one order of magnitude greater than that, it is safe to say that there is room enough in the assigned space to fit the components necessary for the MAV to operate.

The equations to obtain the moment of inertia of a cylinder around the different axes are readily obtained from most classical mechanics textbooks [22]. The mass is considered to be uniformly distributed. The moments are taken with respect to a reference frame placed at the centre of mass of the cylinder, being the x-axis parallel to the axis of revolution:

$$I_x = 8.4816 \times 10^{-5} \tag{3.33a}$$

$$I_y = I_z = 1.3076 \times 10^{-4} \tag{3.33b}$$

It has to be determined where to place the centre of mass. It will be on the plane of symmetry, at a distance x_{cg} from the wing leading edge.

The centre of pressure is the point x_{cp} where the aerodynamic moment is zero, so placing the centre of mass in such point means that the vehicle will not have angular acceleration. Since *AeroFlaps* output moment is taken with respect to the leading edge, which corresponds with the origin of the body fixed reference frame:

$$M_{LE}(t) = x_{cp}L(t) = 0 \rightarrow x_{cp}(t) = -\frac{M_{LE}(t)}{L(t)} \tag{3.34}$$

Since forces are changing with time, there is an instantaneous centre of pressure that is moving. Therefore, it is not possible to choose a centre of mass coincident with the centre of pressure at all instants of time, since centre of mass should not move Therefore, we place the centre of mass at a point such that the integral of moment during a cycle is zero. This means that after some pitch oscillations the vehicle could potentially return to the orientation that it had at the beginning of the cycle. To find such a point, the moment has to be integrated over a whole cycle leaving the $\overline{x}_{cp}$ coordinate as unknown.

$$\begin{aligned} M_x(t) &= M_{LE}(t) + \bar{x}_{cp}L(t) \\ \int_0^T M_x(t)\mathrm{d}t &= \int_0^T M_{LE}(t)\mathrm{d}t + \bar{x}_{cp}\int_0^T L(t)\mathrm{d}t \\ \bar{x}_{cp} &= -\frac{\int_0^T M_{LE}(t)\mathrm{d}t}{\int_0^T L(t)\mathrm{d}t} = 0.367c = 0.0378\ m \end{aligned} \tag{3.35}$$

Therefore, the centre of mass of the body should be placed at a distance $\bar{x}_{cp} = 0.0378\ m$ from the wing leading edge root. From now on that point will be designated as x_{cg}

3.8 Initial conditions for pitch evolution with *AeroFlaps*

From the moment obtained from the code, a preliminary evolution of the motion can be computed by double integration of Newton's second law. The forces will be applied as they were obtained from the vehicle with fixed flight velocity and orientation and with prescribed wing motion. This is a first approximation to the motion evolution. With *DyMoFlaps* the forces will be different once the orientation and velocity change, so it will be more complicated to analyse.

Being M_{cg} the moment applied to the centre of gravity:

$$M_{cg} = I_y\frac{\mathrm{d}^2\theta}{\mathrm{d}t^2} \tag{3.36}$$

This equation needs two initial conditions, $\theta(0)$ and $\dot{\theta}(0)$. By integrating equation (3.36) once it can be shown that the zero net moment during a cycle only ensures

that the angular speed will be the same at the end of the cycle.

$$\int_0^T \frac{M_{cg}(t)}{I_y}\mathrm{d}t = \dot{\theta(T)} - \dot{\theta}(0) = 0 \Rightarrow \dot{\theta}(T) = \dot{\theta}(0) \tag{3.37}$$

However, that does not guarantee that the integral of the angular velocity during the cycle will be zero, only that the velue will be periodic. The integral of the angular velocity equal to zero can be achieved by finding the proper initial angular velocity $\dot{\theta}(0) = \dot{\theta_0}$ that fulfils that condition. By integrating equation (3.36) from 0 to t:

$$\int_0^t \frac{M_{cg}(\tau)}{I_y}\mathrm{d}\tau = \dot{\theta}(t) - \dot{\theta}(0) \rightarrow \dot{\theta}(t) = \dot{\theta}_0 \int_0^t \frac{M_{cg}(\tau)}{I_y}\mathrm{d}\tau \tag{3.38}$$

By integrating the last expression over a period, imposing the cyclic pitch condition $\theta(T) = \theta(0)$ and solving for $\dot{\theta_0}$ the initial angular velocity can be obtained:

$$\int_0^T \left(\dot{\theta}(t) = \dot{\theta}_0 + \int_0^t \frac{M_{cg}(\tau)}{I_y}\mathrm{d}\tau\right)\mathrm{d}t \rightarrow \cancel{\theta(T) - \theta(0)} = \dot{\theta}_0 T + \int_0^T \int_0^t \frac{M_{cg}(\tau)}{I_y}\mathrm{d}\tau\mathrm{d}t$$

$$\dot{\theta_0} = -\frac{1}{I_y T}\int_0^T \int_0^t \frac{M_{cg}(\tau)}{I_y}\mathrm{d}\tau\mathrm{d}t = -1.9737\ rad/s \tag{3.39}$$

The value for the initial condition $\theta(0)$ can be set to obtain an average value of $\overline{\theta} = 0$. For that purpose, the expression for $\theta(t)$ has to be integrated over a period and set to zero.

$$\theta(t) = \theta(0) + \dot{\theta}_0 t + \int_0^t \int_0^\tau \frac{M_{cg}(\tau')}{I_y}\mathrm{d}\tau'\mathrm{d}\tau$$

$$\int_0^T \theta(t)\mathrm{d}t = \int_0^T \theta_0 \mathrm{d}t + \int_0^T \dot{\theta}_0 t\mathrm{d}t + \int_0^T \int_0^t \int_0^\tau \frac{M_{cg}(\tau')}{I_y}\mathrm{d}\tau'\mathrm{d}\tau\mathrm{d}t = 0$$

$$\theta_0 = -\frac{1}{T}\left[\dot{\theta}_0 \frac{T^2}{2} + \int_0^T \int_0^t \int_0^\tau \frac{M_{cg}(\tau')}{I_y}\mathrm{d}\tau'\mathrm{d}\tau\mathrm{d}t\right] = -0.0645\ rad = -3.70^o \tag{3.40}$$

The resulting pitch angle obtained integrating equation(3.36) with the computed initial conditions are shown in Fig. 3.8. Now that the periodic motion has been obtained with the simplified approach, and that an idea of the order of magntude of the oscillations has been obtained, it is time to start using *DyMoFlaps* to obtain the final results.

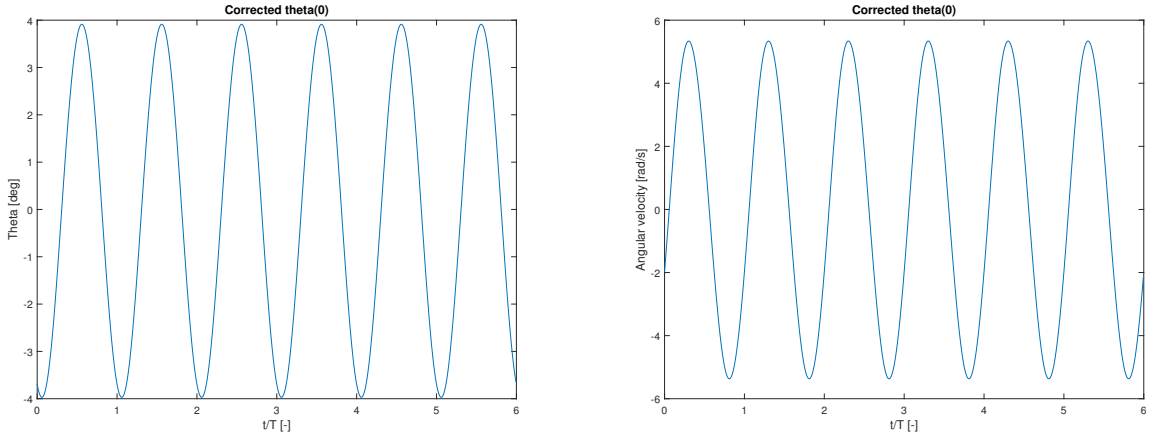

(a) Pitch angle (b) Pitch angular velocity

Figure 3.8: *AeroFlaps* MAV evolution pitch motion estimation

Chapter 4

Straight Level Flight

After the vehicle has been designed, the code designed to compute its motion will be used. Since the motion is free, instantaneous flow field around the wings will not be the same as in the previous computations, where the vehicle was clamped. This is the essential difference between both codes. The first one was used to size the vehicle, but the second one is necessary to assess its performance.

4.1 DyMoFlaps

This program uses the forces computed by *AeroFlaps* to compute the motion of the vehicle. In Fig. 4.1, the algorithm of the program is described with a flowchart. As it can be seen, it includes kinematic integration with the use of quaternion rotation between each time step of *DyMoFlaps*.

On top of the variables that were used in *AeroFlaps*, this code needs

- A value for the drag coefficient has to be introduced to account for the body. The value used will be $C_D = 0.5\frac{\pi}{8}$ (being the wing surface the reference surface), half of the value used on the previous chapter. That is to account for the reduced thrust due to the free motion and reduced speed. The final velocities once the periodic motion was reached were around 93-95% of the design value of $U_\infty = 10\ m/s$

- A complete set of initial conditions for the position, angles, linear velocity and angular velocity.

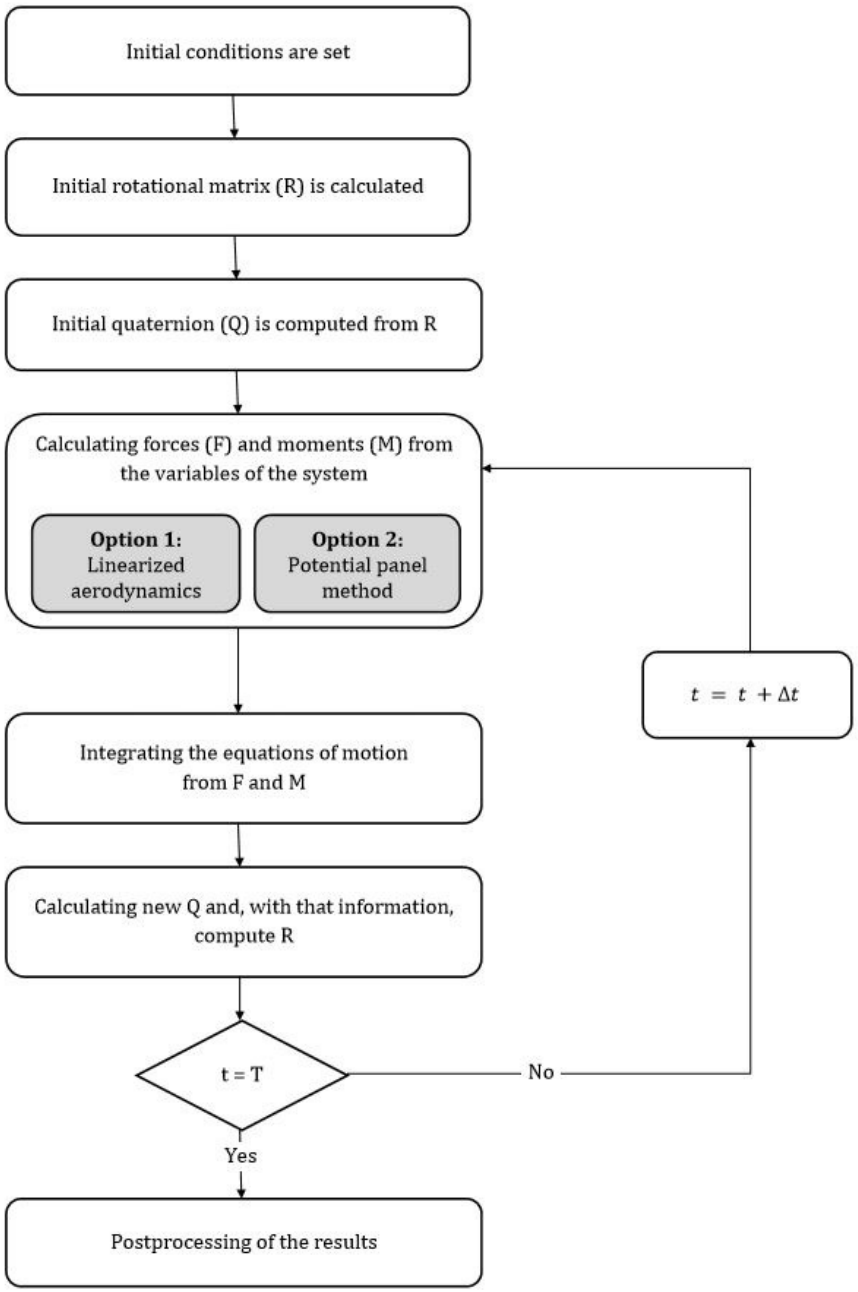

Figure 4.1: Flowchart describing the algorithm in *DyMoFlaps*. The usage of *AeroFlaps* to compute the forces corresponds to ***Option 2**: Potential panel method*

- In addition to the initial conditions, it is necessary to have a file with addition data to start the simulation. That file contains information about the position of the wake panels, the circulation on each wake panel, the circulation on each wing panel and the forces expected for that time step. Those values can be estimated with a *AeroFlaps* simulation.
- Simulation time.

On top of that, the tail model has to be implemented in accordance with the vehicle. This is the aim of this chapter and it serves to the ultimate goal of this project, which is to stabilise the pitching motion of a MAV.

4.1.1 Horizontal flight

The flight path angle is defined as the angle between the trajectory that follows the centre of gravity of the vehicle and the horizontal. The horizontal reference will be the plane perpendicular to the direction of gravity, the plane IXY composed by the inertial X and Y axes. Being V_x and V_y the components of the velocity in expressed in the inertial reference frame:

$$\tan\gamma = \frac{\mathrm{d}y}{\mathrm{d}x} = \frac{V_y}{V_x} \tag{4.1}$$

Due to the unsteadiness of the forces, the centre of gravity of the vehicle will oscillate up and down. This means that the instantaneous value of the flight path angle may not give information about the overall trajectory. In order to have a meaningful definition of this parameter, the flight path angle will be obtained by computing the difference in position between the same instant of two different periods:

$$\gamma(t) = \arctan\left(\frac{z(t) - z(t-T)}{x(t) - x(t-T)}\right) \tag{4.2}$$

where T is the flapping period. From the equations of motion for flight on a vertical plane, another definition for the flight path angle can be obtained [23].

$$T - D - W\sin\gamma = 0 \Rightarrow \gamma = \sin^{-1}\left(\frac{T-D}{W}\right) = \sin^{-1}\left(\frac{\overline{T}-\overline{D}}{W}\right) \tag{4.3a}$$

$$\overline{L} - W\cos(\gamma) = 0 \tag{4.3b}$$

where the forces are shown as cycle averaged. From the equations (4.3) it is made clear that thrust must overcome the drag in order not just to maintain speed, but also altitude.

In the previous chapter stable pitch oscillations were obtained without a tail. This was possible because the moment was a predetermined function which is no longer possible. Therefore, a residual climb angle will be present. The purpose of this project is to damp pitch oscillations, which is still something that can be analysed when the vehicle is climbing, especially when the residual climb angle might be of the order of $\gamma = 0.1^o$. The dynamics are essentially the same as for a truly levelled flight.

Flight path angle for each simulation presented on this document will include the flight path angle exhibited after the periodic oscillations are obtained. It will be computed as shown in equation (4.2).

4.2 Flight with no tail

To begin with the simulations, the vehicle without a tail with the conditions that achieved periodic pitch oscillations will be tested.

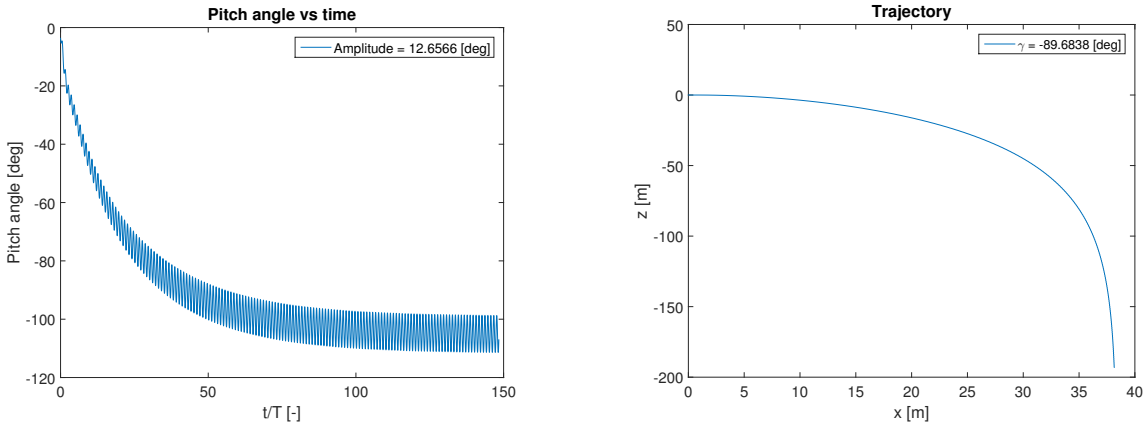

(a) Pitch angle

(b) Trajectory

Figure 4.2: *DyMoFlaps* MAV evolution without tail. Same initial conditions as in Fig. 3.8

As shown in Fig. 4.2, the vehicle is not able to maintain flight with no tail installed. To achieve a stable oscillation, the net moment integral around the centre of mass during a cycle has to be zero. The centre of mass was placed at the point where *AeroFlaps* predicted this condition to be fulfilled, but since the forces changed, the net moment integral around the fixed centre of gravity is not zero anymore.

There might be a way to obtain horizontal flight with appropriate initial conditions, but it would require an iterative process. Furthermore, the result would be

impractical since any slight distortion of the initial conditions would cause the vehicle to quickly evolve into erratic motion as in this example. A tail device is therefore necessary.

4.3 Tail wing model

The first stabilisation method to be studied is a fixed tail. In order to do so, a tail geometry has to be defined. The tail wing is modelled using XFLR5, a program for airfoil and wing design analysis. The effectiveness of aerodynamic tail devices is usually measured in terms of the volume tail ratio:

$$V_H = \frac{l_t}{c}\frac{S_t}{S_w} \tag{4.4}$$

where l_t is the distance from x_{cg} to the tail leading edge[1], c_w is the chord of the main wing, and S_t and S_w are the tail surface and wing surface, respectively. The parameter considers the fact that increasing the tail distance has the same impact as increasing the tail wing surface in term of moments. In that way, it is desirable to have a small tail placed far away from the body because less drag is produced. Furthermore, having a big forces on the tail would affect the linear motion of the centre of gravity. However, having a very small tail surface has its limitations. The rigid element connecting the tail with the body would become too heavy as more length is required. A balance between the two of the parameters is required to obtain a feasible vehicle. The values will be determined later, after the tail aerodynamic model is known.

4.3.1 XFLR5 analysis

The tail, to be designed with XFLR5, will be composed of one rectangular surface with no sweep or twist. The airfoil will be NACA0012. The aspect ratio will be $AR_t = AR_w = 2$. An analysis was performed to obtain tabulated values for C_L, C_D, $C_{My_{LE}}$ as a function of the angle of attack, ranging from -19.5 to 20 degrees in increments of 0.5^o. The coefficients obtained are tabulated on Appendix A.

To obtain the values of the coefficients based on tabulated information, linear interpolation would be used. Since the value of the angle of attack of the tail will

[1]Usual formulation considers the distance from vehicle centre of gravity to the aerodynamic centre of the tail. However, since the moment of our tail model is taken from the leading edge, the distance will be chosen accordingly

change on every time stem, interpolation on every step would increase the computational cost significantly. To avoid that, polynomial fitting has been used to obtain the aerodynamic coefficients as an analytic function of the angle of attack. As can be read on any classical aerodynamics textbook[24], the lift and moment coefficients depend linearly on the angle of attack, while the drag follows a quadratic function. Since the airfoil is symmetric and potential theory is used, aerodynamic forces and moments are zero at $\alpha_t = 0$. The polinomials obtained after the fitting are the following:

$$C_{L_t}(\alpha) = C_{L_{t,0}} + C_{L_{t,\alpha}}\alpha = 2.4875\alpha \tag{4.5a}$$

$$C_{M_t}(\alpha) = C_{M_{t,0}} + C_{M_{t,\alpha}}\alpha = -4.4860\alpha \tag{4.5b}$$

$$C_{D_t}(\alpha) = C_{D_{t,0}} + C_{D_{t,\alpha^2}}\alpha^2 = 0.9518\alpha^2 \tag{4.5c}$$

Those coefficients are loaded into the program to compute the tail forces at each time step.

4.3.2 *DyMoFlaps* tail integration

To compute the forces produced by the tail, the local angle of attack of the tail needs to be computed. Body-fixed axes will be used to compute it. The velocity that the tail sees is the sum of the flow velocity (expressed in body-fixed axes) and the relative velocity due to the rotation around the centre of mass, as depicted in Fig.4.3.

$$\vec{V}_{tail}|_b = \vec{V}_{flow}|_b + (0, 0, ql_t) \tag{4.6}$$

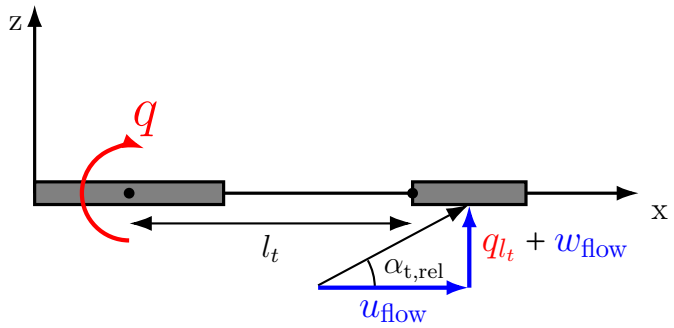

Figure 4.3: Tail angle of attack

so the angle of incidence of the flow with the tail is:

$$\alpha_{t,rel}(t) = \arctan\left(\frac{w_{flow}|_b + l_t q}{u_{flow}|_b}\right) \tag{4.7}$$

This angle of incidence will tilt the resulting forces since, by definition, the lift is perpendicular to the incident velocity. The lift and drag of the tail can be rotated into contributions to forces F_x and F_z on body-fixed reference frame.

$$F_z = L_t \cos(\alpha_{t,rel}) + D_t \sin(\alpha_{t,rel}) \tag{4.8a}$$

$$F_x = -L_t \sin(\alpha_{t,rel}) + D_t \cos(\alpha_{t,rel}) \tag{4.8b}$$

To compute the forces, the mounting angle of the tail has to be added. It does not affect the direction of the forces, only its magnitudes.

$$\alpha_t = \alpha_{t,0} + \alpha_{t,rel} \tag{4.9}$$

$$L_t = L(\alpha_t) = 2.4875\alpha_t \frac{1}{2}\rho U_\infty^2 S_t \tag{4.10a}$$

$$M_t = M(\alpha_t) = -4.4860\alpha_t \frac{1}{2}\rho U_\infty^2 S_t c_t \tag{4.10b}$$

$$D_t = D(\alpha_t) = 0.9518\alpha_t^2 \frac{1}{2}\rho U_\infty^2 S_t \tag{4.10c}$$

4.4 Fixed mounting angle

The moment produced by the tail should be able to counteract the moment around the centre of mass. To have an estimation of the mounting angle, the moment acting on the centre of mass should be considered. However, the centre of mass has (ideally) an integrated moment equal to zero. Although it is known that that point will have a nonzero net moment on this simulation, it cannot be anticipated. A way to estimate $\alpha_{t,0}$ for the first simulation is to use the moment about the leading edge, $\overline{M}_{x_{LE}}$ obtained from *AeroFlaps*.

Equilibrium of moments will be applied to match the moment with no tail to the moment that a tail would produce, so that the angle of attack resulting from imposing that condition is sufficient to counteract it.

$$\overline{M}_{tail} = -l_t \overline{L}_t \tag{4.11}$$

$$\overline{M}_{x_{LE}} + \overline{M}_{tail} = 0 \Rightarrow \overline{M}_{x_{LE}} = l_t \overline{L}_t \Rightarrow \frac{\overline{M}_{x_{LE}}}{\frac{1}{2}\rho U_\infty^2 S_w c_w} = \frac{\overline{L}_t}{\frac{1}{2}\rho U_\infty^2 S_t} \frac{l_t}{c_w} \frac{S_t}{S_w} \tag{4.12}$$

Recall that the quotient at the end of the previous expression is the volume tail ratio, defined in equation (4.4). Therefore the expression for $\alpha_{t,0}$ needs a value for that parameter:

$$\overline{C_{M_{x_{LE}}}} = C_{L_{t,\alpha}} \alpha_{t,0} V_H \Rightarrow \alpha_{t,0} = \frac{\overline{C_{M_{x_{LE}}}}}{C_{L_{t,\alpha}}} V_H^{-1} \tag{4.13}$$

The angle required is inversely proportional to the volume tail ratio. The stronger the tail moment(because it is bigger or further away), the smaller is the angle required to fulfil the condition.

There are two undefined variables related by one equation. One of them has to be decided. Defining sensible values for the arm length and tail surface to obtain a volume tail ratio (and later the mounting angle) is more convenient than selecting and arbitrary mounting angle and having to adapt the tail for it. The tail surface selected is half the corresponding to half of one wing:

$$S_t = \frac{S_w}{2} = 0.0106\ m^2 \Rightarrow \frac{S_t}{S_w} = 2 \tag{4.14}$$

The tail distance will be determined by a distance of 5 wing chords, measuring from the wing leading edge to the tail leading edge. Since the value l_t is the distance from the centre of mass, and x_{cg} is the distance from the leading edge to the centre of mass:

$$l_t = 5c_w - x_{cg} = 0.4771\ m \Rightarrow \frac{l_t}{c_w} = 5 - \frac{x_{cg}}{c_w} = 4.6333 \tag{4.15}$$

The final volume tail ratio is:

$$V_H = 2.317 \tag{4.16}$$

From plugging into (4.13) the corresponding values from equations (4.5) and (4.16):

$$\alpha_{t,0} = \frac{-0.2724}{2.4875} 2.317^{-1} = -0.0472\ rad = -2.72^o \tag{4.17}$$

Now that the tail is completely defined, a simulation with the preliminary value for the mounting angle can be computed. The simulation inputs will be composed of those showed on Table 3.2 as well as the initial conditions and the *DyMoFlaps* specific variables defined on this chapter, on Table 4.1.

$C_{L_{t,\alpha}}$ $[-]$	2.4875	$C_{D_{t,\alpha^2}}$ $[-]$	0.9518
$C_{M_{t,\alpha}}$ $[-]$	−0.4860	C_D $[-]$	$0.5\frac{\pi}{8}$
c_t $[m]$	0.0728	AR_t $[-]$	2
(x_0, y_0, z_0) $[m]$	$(0, 0, 0)$	(u_0, v_0, z_0) $[m/s]$	$(10, 0, 0)$
θ_0 $[rad]$	−0.0645	$\dot{\theta}_0$ $[rad/s]$	−1.9737
l_t $[m]$	0.4771	$\alpha_{t,0}$ $[rad]$	−0.0475

Table 4.1: Values for the variables and initial conditions of the *DyMoFlaps* simulation

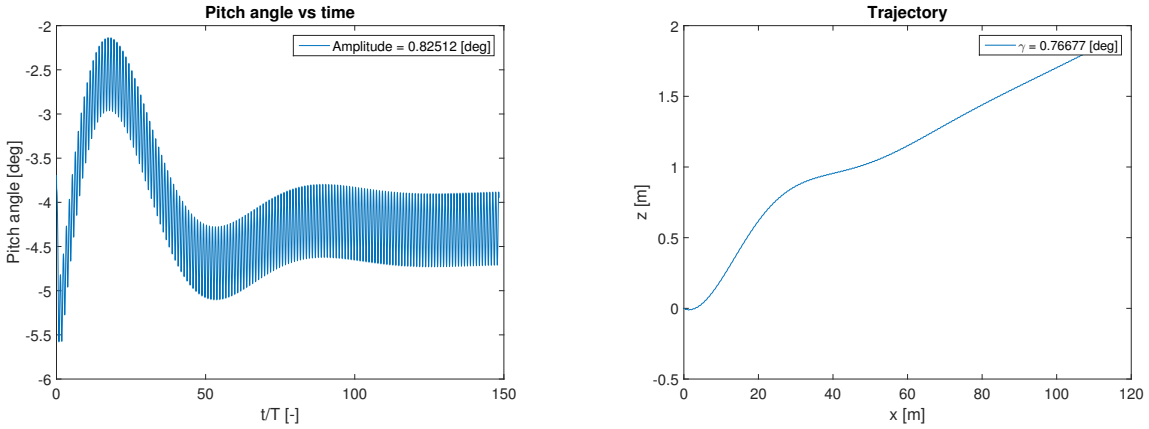

(a) Pitch angle (b) Trajectory

Figure 4.4: Motion with fixed tail at $\alpha_{t,0} = -2.72^o$. Initial conditions estimated with *AeroFlaps*

Simulation resulting pitch oscillations are shown on Fig. 4.4a. The transient behaviour before the periodic oscillations is the consequence of using initial conditions that do not correspond to the final cyclic forces when using this program. Because of that transient, the oscillations of the final cyclic state are centred around $\theta = -4.3^o$. Another simulation with every initial condition equal to zero (except the forward velocity) will be computed to check the behaviour. The results are plotted in Fig. 4.5 and show that there is another stable mean pitch angle, at $\theta = 3.1^o$.

Fig 4.4b shows the trajectory followed by the vehicle. The resulting value of the climb angle is $\gamma = 0.75^o$, which could be reduced. In order to obtain a trajectory closer to horizontal, a new simulation is performed with $\alpha_{t,0} = -2.5^o$.

The new simulation is shown in Fig. 4.6. The pitch oscillations are similar, but with a smaller mean value. Since the pitch-up moment caused by the tail is reduced, the vehicle orientation (as well as trayectory with $\gamma = 0.187^o$) is more aligned with

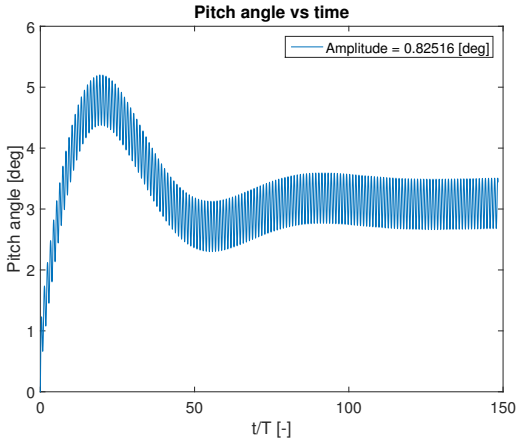

(a) Pitch angle

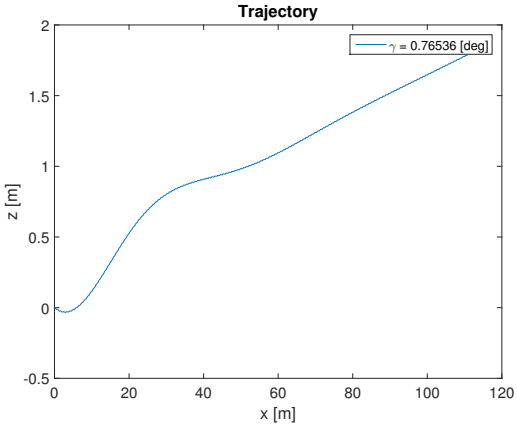

(b) Trajectory

Figure 4.5: Motion with fixed tail at $\alpha_{t,0} = -2.72^o$. Initial conditions equal to zero

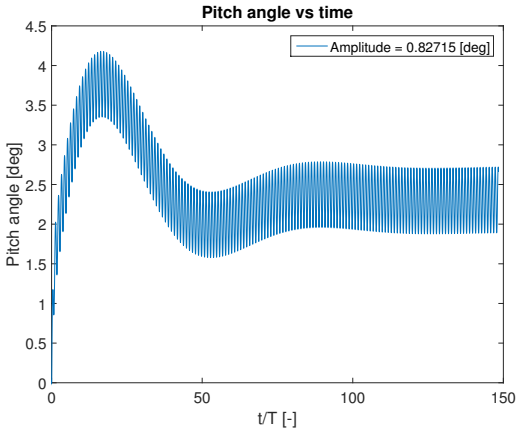

(a) Pitch angle

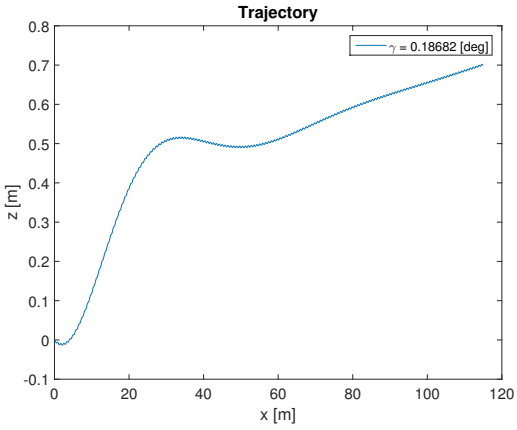

(b) Trajectory

Figure 4.6: Motion with fixed tail at $\alpha_{t,0} = -2.5^o$. Initial conditions other than u_0 set to zero.

the horizontal.

The results from the last simulation, with this set of tail geometrical parameters corresponding to $\alpha_{t,0} = -2.5^o$, will be used as basis for the open loop control developed on the next chapter.

The initial conditions and wake initiation file will be updated to match the behaviour at the end of the last simulation (Fig. 4.6), so that the transient motion at the beginning of each simulation on the following sections is greatly damped. This will allow shorter simulations to reach equally cyclic behaviour.

To make the stored condition valid for the start of the next simulation at $t = 0$, the instant at which the information is recorded must have the wings at the same position and velocity as for $t = 0$. That instant will be $t = nT$, being n the biggest integer possible without exceeding the simulation time, and T is the flapping period.

4.5 Mobile tail: Open Loop

Variable angle tail can further reduce the pitch oscillations by adapting the mounting angle to produce different moment depending on the instantaneous conditions of the vehicle. It has the disadvantage of increasing the Operative Empty Weight of the vehicle, since the mechanism that allows rotation has to be added, as well as the additional control system, power transmission from the power unit to the tail, and the tail actuator.

The payload and oscillation amplitude trade-off should be decided based on the vehicle mission. For a transport MAV, the increased payload would be more important that some additional pitch damping. For a vehicle carrying a camera, the additional weight to make the pitch smoother may be worth it as long as there is weight credit enough for the desired camera.

This project does not answer to a particular mission. Its purpose is to study the different ways to damp the pitch oscillations of a flapping-wing MAV, and for that reason the mobile tail control will be studied. Its implementation would be a design option for each individual vehicle based on its particular mission.

4.5.1 Tail deflection estimation

To obtain an estimation of the tail additional deflection that should be added (or subtracted) to the fixed mounting angle, it should be computed to counteract the moment during a cycle of the stabilised motion obtained on last section. That moment, $M_{fix}(t)$ is plotted on Fig. 4.7.

The aim of the tail additional deflection is to make the total moment on the vehicle zero at any instant of time. Considering that the moment $M_{fix}(t)$ remains unchanged:

$$M_{fix}(t) + M_{OL}(t) = 0 \Rightarrow M_{OL}(t) = -M_{fix}(t) \tag{4.18}$$

Following a procedure analogous to that of equations (4.12) and (4.13), a function

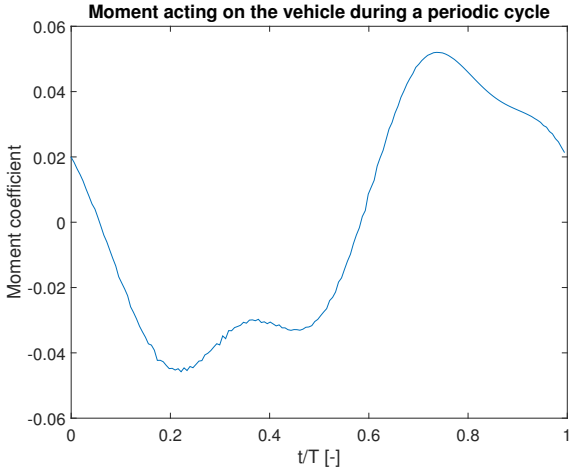

Figure 4.7: Moment acting on the vehicle during a cycle with fixed tail flight

for the angle of attack can be computed:

$$\Delta\alpha'_{t,OL}(t) = \frac{C_{M_{OL}}(t)}{C_{L_{\alpha,t}}} V_H^{-1} \tag{4.19}$$

The resulting function is similar to a sine function. It may be convenient in terms of control system and power transmission implementation to define a sine function in such a way that the resulting moment produced is the same.

$$\Delta\alpha_{t,OL}(t) = A\sin(\omega t) \tag{4.20a}$$

$$A = \max(\Delta\alpha'_{t,OL}(t)) \tag{4.20b}$$

That function does not guarantee that the moment caused by the sinusoidal tail motion will be the same as the one obtained in equation (4.19). That condition can be imposed by multiplying the sinusoidal function by a constant and solving for the value that makes the cycle integral of the moment equal.

$$\int_0^T \Delta\alpha'_{t,OL}(t)\mathrm{d}t = C\int_0^T \Delta\alpha_{t,OL}(t)\mathrm{d}t \Rightarrow C = \frac{\int_0^T \Delta\alpha'_{t,OL}(t)\mathrm{d}t}{\int_0^T \Delta\alpha_{t,OL}(t)\mathrm{d}t} \tag{4.21}$$

In Fig. 4.8, the preliminary and the adapted tail deflection functions are shown.

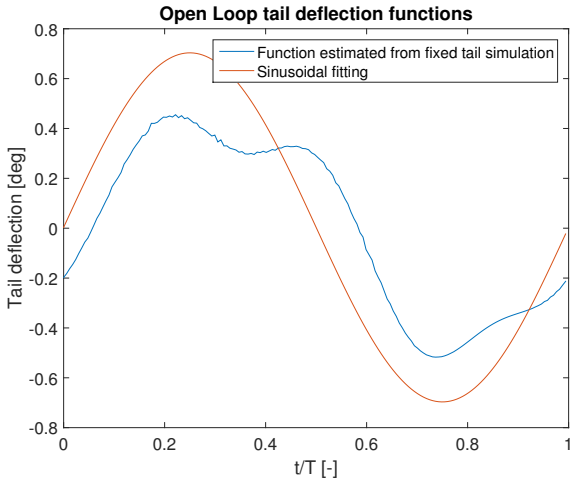

Figure 4.8: Moment acting on the vehicle during a cycle with fixed tail flight

4.5.2 Simulation results

The flight controlled with Open Loop is simulated. The only difference with respect to the fixed tail simulation is the value for the angle of attack of the tail:

$$\alpha_t(t) = \alpha_{t,0} + \alpha_{t,rel}(t) + \Delta\alpha_{t,OL}(t) \tag{4.22}$$

In Fig. 4.9 the simulations with open loop control are plotted together with the fixed tail flight. The same initial conditions and wake startup were used for both cases.

The open loop control does not offer significant damping to the oscillations, although a slight reduction on the amplitude is observed when compared to fixed tail. The sinusoidal fitting proved to be more effective than the directly obtained from the moment equation.

In order to find a way to get the most out of the open loop control, several ways to operate the tail will be tested:

- Varying the deflection amplitude.
- Phase shift of the tail deflection with respect to the wing flapping.
- Step-wise deflection

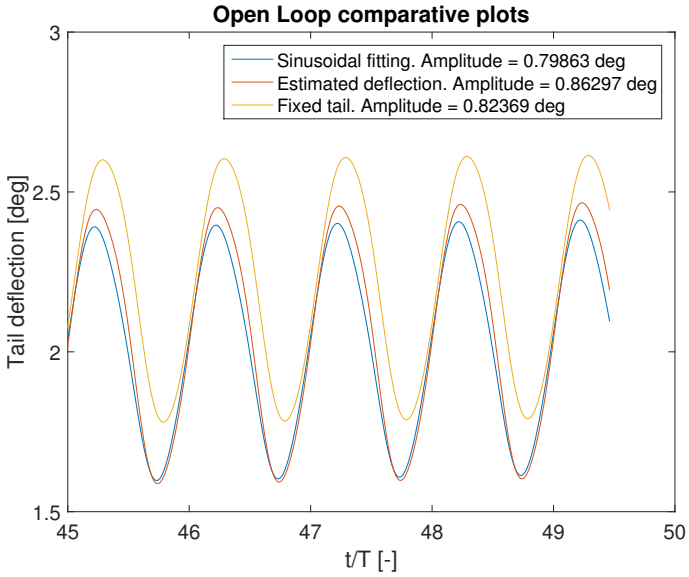

Figure 4.9: Open Loop control and fixed tail

Deflection amplitude

Incresing the amplitude of the deflection may enhance the damping capability of the tail. In order to assess if such assumption is true, a new tail motion is defined based on the former sinusoidal function:

$$\Delta\alpha^{k}_{t,OL}(t) = k\Delta\alpha_{t,OL}(t) \tag{4.23}$$

the values of k used for this simulations are $k = 0.5, 1, 2, 4$. A reduced value below one is included to check if the problem was an excessive deflection. On Fig. 4.10, the starting first cycles as well as the periodic state are compared between the different simulations.

The results show that there is some damping when using $k = 0.5, 1$, but the amplitude of the oscillations increases as the tail deflection is increased further than that. It also causes a shift on the clycles.

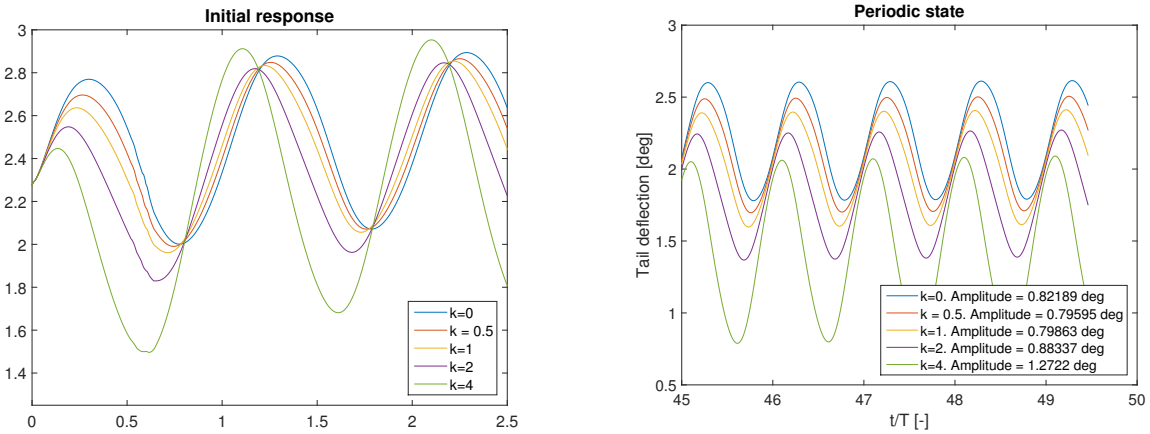

(a) First cycles (b) Periodic state

Figure 4.10: Pitch angle evolution for different tail deflection amplitude.

Step deflection

This method consists on setting the deflection to either the maximum or minimum value, without intermediate values:

$$\Delta\alpha_{t,OL}^{step}(t) = \max(\Delta\alpha_{t,OL}(t)) \quad \text{if} \Delta\alpha_{t,OL}(t) >= 0 \tag{4.24a}$$

$$\Delta\alpha_{t,OL}^{step}(t) = \min(\Delta\alpha_{t,OL}(t)) \quad \text{if} \Delta\alpha_{t,OL}(t) < 0 \tag{4.24b}$$

This approach did not show to be any better than the preious ones.

Phase shift

Another parameter that can be modified in order to damp the pitch oscillations of the vehicle is the tail deflection delay with respect to the wing motion. Phase shifts $\phi_t = \pm 90^o$ will be applied to the tail deflection sinusoidal function. Retaking the formulation from 4.20:

$$\Delta\alpha_{t,OL}^{\phi}(t) = A\sin(\omega t + \phi_t) \tag{4.25}$$

As it can be seen in Fig. 4.12, when the phase shift negative, the oscillations are effectively damped.

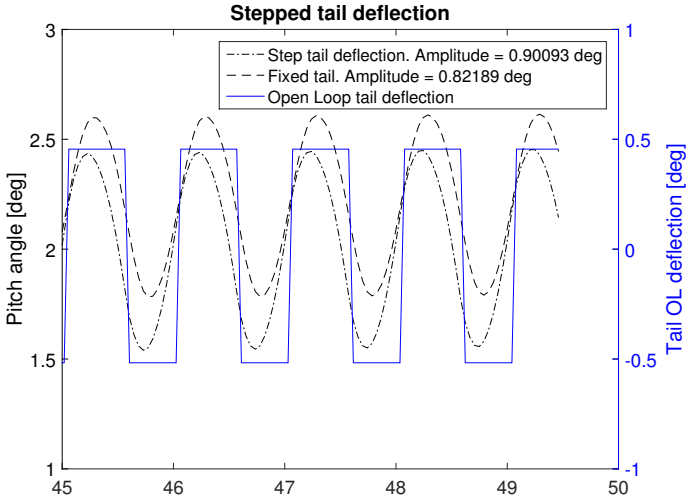

Figure 4.11: Stepped tail deflection with different amplitudes

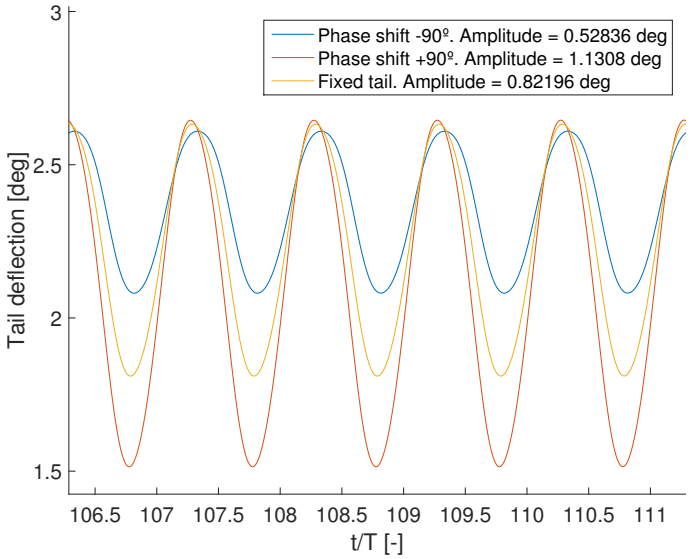

Figure 4.12: Stepped tail deflection with different amplitudes

4.5.3 Open Loop conclusion

The phase between the tail motion and the wing flapping seems to be the key parameter for an Open Loop control system for a flapping wing MAV. However, the

final result could be improved by means of Closed Loop control techniques, as will be studied in the next section.

4.6 Mobile tail: Closed loop

In this section, the effectiveness of controlling the tail by a feedback system is assessed. A closed loop control system uses the information about the output of the system (in this case, information about the motion) that is gathered by the sensors (6 Degree of Freedom sensor including 3-axis accelerometer and gyroscope, for instance) in order to control the vehicle. This offers advantages over the open loop control, such as the possibility to compensate external disturbances. It also has its risks, such as incorrect controller tunning that can lead to overcompensating errors causing unstable or amplified oscillations[25].

A PD controller will be designed. PD controllers require the system error signal as input and give an output based on the error and its time derivative. Defining the error system as the difference between the system state and the reference state:

$$e(t) = \theta(t) - \theta_{ref} \tag{4.26}$$

where θ_{ref} is the mean value of θ during one periodic cycle of the final fixed tail flight. Fig. 4.13 shows how the the PD controller works.

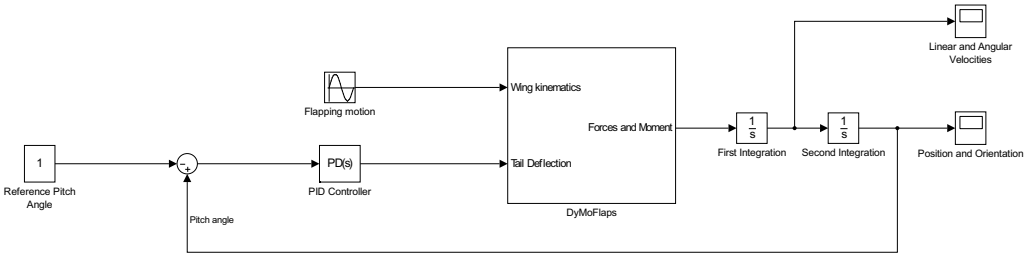

Figure 4.13: Control system block diagram

4.6.1 Sampling frequency

When it comes down to manufacturing, additional difficulties arise. A gyroscope and tail actuator cannot have an instantaneous response and it should be taken into account when dealing with feedback systems working on high flapping frequencies.

The performance of the measurement and actuation systems could be analysed separately. For simplicity, on this analysis in this deflection of the tail will be applied on the immediate time step after the measurement.

A sampling frequency of $f_{samp} = 1000\ Hz$ will be used, but sensitivity analysis of that parameter will be performed by testing the final controller with lower frequencies. This is key since a slow refreshment of the tail deflection may lead to a peak value of the moment acting more time than required, making the system unstable.

4.6.2 Proportional controller

Tuning a PID controller (Including PD controllers, as in this case) is a very experimental procedure, based on following a "trial and error" approach. In order to make this procedure simpler, the proportional term is tuned first (with the other one/two set to zero) to find a suitable value. That value is fixed while the other term or terms of the PID controller are tuned. This is the approach that has been followed.

Based on the estimations made for the Open Loops analysis with help of equation (4.19), it was seen that a peak Open Loop deflection was about $\Delta\alpha'_{t,OL} = 0.6^o$. That was used for simulations where the maximum pitch angle amplitude was of the order of $\theta = 0.8^o$, which means peak errors of $e(t) = \theta - \theta_{ref} = 0.4^o$.

For a proportional controller only:

$$\Delta\alpha_{t_{CL}} = k_p e(t) \Rightarrow k_p = \frac{\Delta\alpha_{t_{CL}}}{e(t)} \approx \frac{0.6}{0.4} = 1.5 \tag{4.27}$$

The sign is positive because to counteract a positive pitch angle, a nose down moment should be created. Such moment is obtained increasing the lift on the tail, and thus increasing the angle of attack of the tail.

On the first simulations with $k_p = 1.5$, the performance didn't seem to change from fixed tail flight. Values from $k_p = 1.5$ to $k_p = 15$ in increments of 1.5 were used to look for an impact on the damping.

On Fig 4.14a, the final state values $k_p = 1.5, 7.5, 15$ after the transient effects die out are plotted together. On Fig 4.14b, the final amplitude of oscillations relation with the value of the proportional controller is shown. It is seen that the influence is very strong. Although the value of the proportional controller gets quite high, the magnitude of the error is below one degree at all instants, so no large deflections are required by the tail. However, for real flight where perturbations could cause a disturbance of several degrees on pitch angle, a saturation value for the tail deflection would be required.

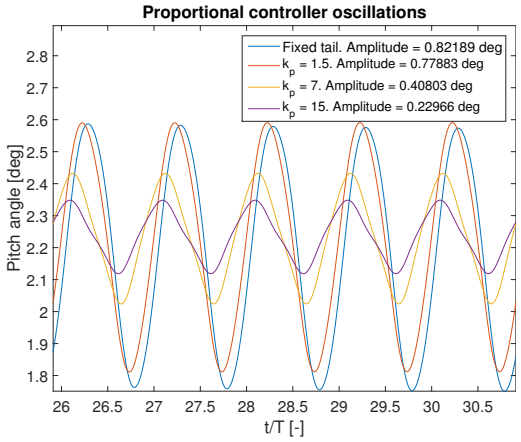

(a) Oscillations with proportional control

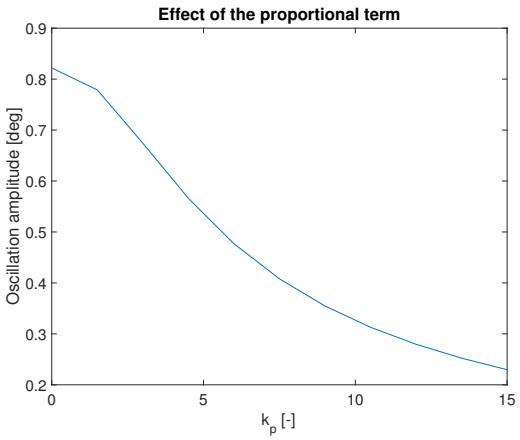

(b) Proportional parameter influence

Figure 4.14: Proportional controller analysis

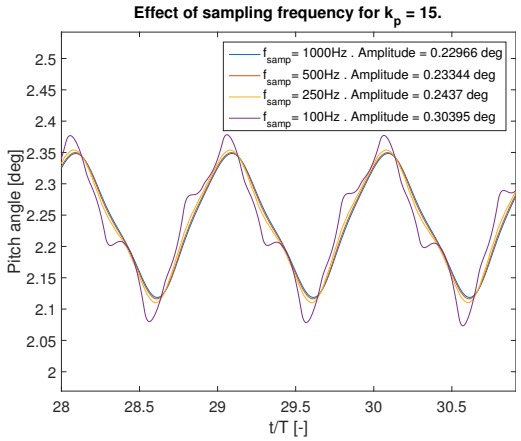

(a) Oscillations with different sampling frequencies

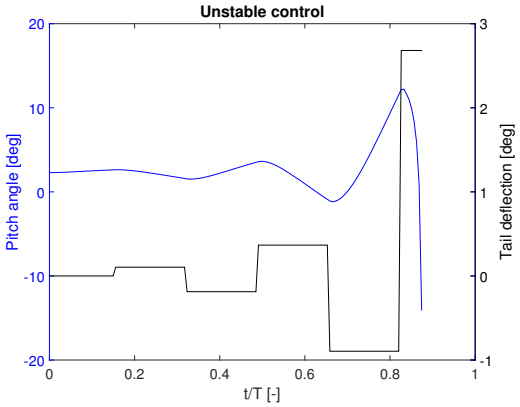

(b) Unstable behaviour

Figure 4.15: Sampling frequency study

The sampling frequency used for the previous simulations was $f_{samp} = 1000\ Hz$. The relevance of this parameter is checked by repeating the simulation with different frequencies. Te results are shown in Fig. 4.15a. As it can be seen, the frequency can be reduced down to $f_{samp} = 100\ Hz$, which is stable but close to the margin. By reducing the frequency below that value, as on the simulation shown in Fig. 4.15b with $f_{samp} = 75\ Hz$, the low feedback rate leads to increasing oscillations.

4.6.3 Proportional-Derivative controller

The derivative term of the controller will be used to further improve the oscillation damping. According to the usual formulation of such controller:

$$\Delta\alpha_{t_{CL}} = k_p e(t) + k_d \frac{\mathrm{d}e(t)}{\mathrm{d}t} \tag{4.28}$$

Notice that the derivative of the error with respect to time is equal to the pitch rate:

$$\frac{\mathrm{d}e(t)}{\mathrm{d}t} = \frac{\mathrm{d}}{\mathrm{d}t}\left(\theta - \theta_{ref}\right) = \frac{\mathrm{d}\theta}{\mathrm{d}t} = q \tag{4.29}$$

In order to get a first value of the derivative term of the controller, the approach followed is to make the weight of the derivative term similar to that of the proportional term (making use of equation (4.29)). The amplitude of the error term on fixed tail simulations is of the order of $e(t) = 0.007\ rad$, while the pitch rate takes values of the order of $q = 0.6\ rad/s$:

$$\frac{k_p e(t)}{k_d \dfrac{\mathrm{d}e(t)}{\mathrm{d}t}} \approx 1 \Rightarrow \frac{k_d}{k_p} \approx \frac{e(t)}{q} \approx 0.0117 \tag{4.30}$$

The final controller equation, making use of equations (4.28) and (4.30), is the following:

$$\Delta\alpha_{t_{CL}} = k_p e(t) + k_d \frac{\mathrm{d}e(t)}{\mathrm{d}t} = k_p \left(1 + \frac{k_d}{k_p}\frac{\mathrm{d}}{\mathrm{d}t}\right) e(t) = 15\left(1 + 0.0117\frac{\mathrm{d}}{\mathrm{d}t}\right) e(t) \tag{4.31}$$

However, that derivative term is just an estimation. In order to check different parameters, a new variable K_D is introduced to vary proportionally the derivative term of the controller:

$$\Delta\alpha_{t_{CL}} = k_p \left(1 + \frac{k_d}{k_p}\frac{\mathrm{d}}{\mathrm{d}t}\right) e(t) = k_p \left(1 + K_D\frac{k_d}{k_p}\frac{\mathrm{d}}{\mathrm{d}t}\right) e(t) \tag{4.32}$$

Fig. 4.16 shows the effect of adding a derivative term to the controller. The oscillations are more damped than with the proportional controller. However, the system becomes more unstable. The simulations shown are performed with a sampling frequency $f_{samp}1000\ Hz$. With $f_{samp} = 500\ Hz$, a frequency that allowed the simulation of the proportional controller without issues, the simulation with $K_D = 1$

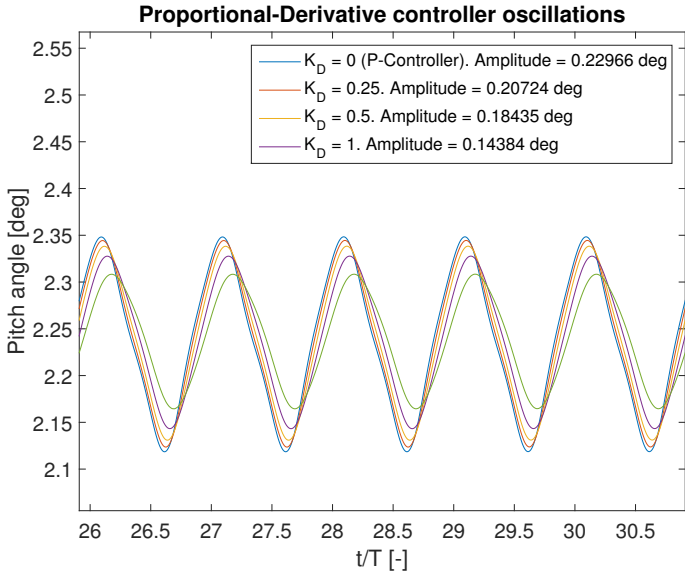

Figure 4.16: Pitch angle evolution under different proportional-derivative controllers

becomes unstable. Furthermore, a simulation keeping the sampling frequency to f_{samp} = 1000 Hz and using K_D = 1.25 becomes unstable too.

The stronger the controller (specially if derivative control is used), the higher the sampling frequency required to avoid running into unstable behaviour. However, the range of oscillation amplitude that this controller is achieving is of the order of $\theta = 0.15^o$. A softer controller with a less demanding sampling frequency would be sufficient for most missions, even if the final amplitude is increased by a few times the value obtained.

4.7 Inertial control

Inertial control is inspired on animals with flexible bodies. By bending the rear end of their bodies, they modify their inertial properties to produce different motion, or to make use of the inertial forces. Together with the different stroke patterns and, in some cases, their aeroynamic tails, is one of the reasons behind their superior manouevrability.

One of the uses of this inertial forces is the damping of the pitch oscillations. In the case of vehicles such as the one defined in this document, the aerodynamic tail could be substituted by an inertial tail device. The geometry proposed is shown on

Fig. 4.17. It consists of a rigid element hinged at the rear end of the fuselage, that would be deflected in order to create a moment:

$$M_{t,inertial} = l_t F_{inertial} = l_t m_t l_t \ddot{\theta}_t = l_t^2 m_t \ddot{\theta}_t \tag{4.33}$$

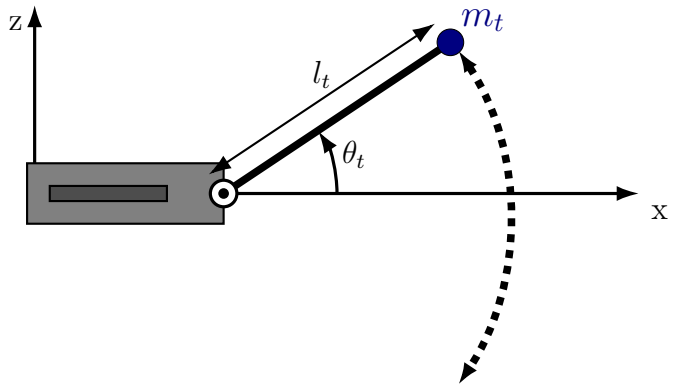

Figure 4.17: Inertial tail device diagram

However, this mechanism has a limitation. In order to be able to continue its operation, it should end the cycle with the tail at the same position than at the beginning. This is only fulfilled as long as the integral of the moment caused by the inertial tail is zero. However, if the aim is to substitute the aerodynamic tail with an inertial one, this is not acceptable. Whilst the moment on the vehicle has a moment integral equal to zero on a cycle, this is because the body and the aerodynamic tail contributions cancelled each other, but none of them was zero. Because of this, an inertial tail cannot substitute the aerodynamic tail directly.

What can be assessed is the capability of the inertial tail to damp the oscillations caused. One way to do this is to analyse the moment as a deviation from its mean value, a "perturbation moment". That way, the inertial tail would act to counteract the instantaneous moment during the cycle, being the cyclic integral of the "perturbation moment" equal to zero. This approach is the equivalent to having a fixed aerodynamic tail (that contributes with a nonzero moment integral to counteract the net moment contribution of the body) with the added inertial mechanism. However, the purpose of this section is not to design a specific mechanism, but to make an order of magnitude analysis of the masses/deflections that would be needed to for an inertial tail to create the moments required to damp the moments causing oscillations.

From the moment of a cycle with fixed tail and applying the procedure described on the last paragraph. The tail angular deflection acceleration is obtained by solving

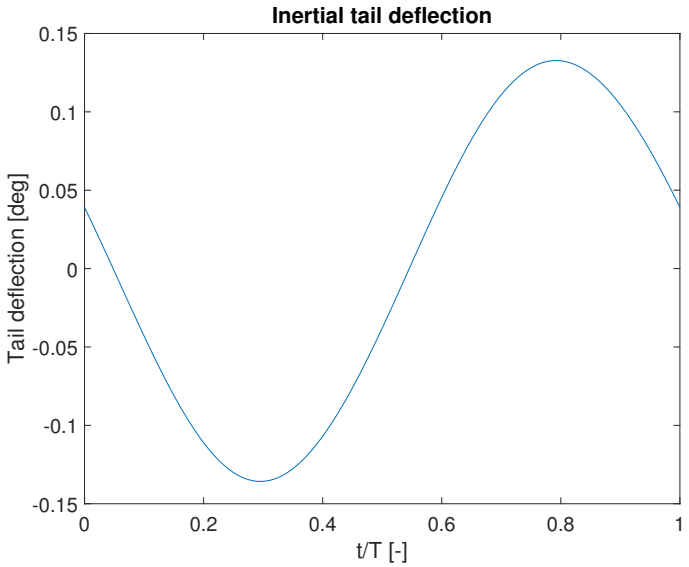

Figure 4.18: Inertial tail deflection to cancel moment fluctuations. $m_t = 0.1m$

equation (4.33) for $\ddot{\theta}$, and imposing a moment equal to the one recorded from the simulation with an aerodynamic tail, M_{aero}:

$$\ddot{\theta}(t) = \frac{M_{aero}(t)}{l_t^2 m_t} \tag{4.34}$$

On Fig. 4.18 is plotted the deflection required to damp the vehicle oscillations, when an equivalent to 10% of the mass of the body is placed at the tail. The angular acceleration caused by these moments on a body with a moment of inertia as small as this one is of the order of $\ddot{\theta} = 20\ rad/s^2$, but to convert that acceleration into an angular displacement, a double integration in time is performed. Being the period of this vehicle in particular so fast, there is no time for those relatively big moments to require significant tail deflections.

Chapter 5

Conclusion and future work

5.1 Summary

In this project, the procedure of design of a flapping-wing MAV from zero was developed step by step. Since this technology is on an early stage compared to other aerial vehicles such as rotatory-wing and fixed-wing aircraft, most of the inspiration and order of magnitude considerations came directly from nature, being bats, birds and insects the reference flappers, with their unmatched performance after all their years of evolution. After the vehicle was developed, the focus was put on damping the pitch oscillations as much as possible by means of several approaches: fixed and mobile aerodynamic tails as well as the inertial tail.

From the design process, the parameters correlations obtained from nature observation showed to be key for the selection of several parameters. It was observed that the wings flapping in a pitch and flap combination have the generation of horizontal and vertical force more decoupled that one might have expected. Although both forces are generated by the motion of the wing, the flap amplitude has an strong effect on the thrust while the pitch angle modelling mostly determines the lift, being the phase between the two motions key to allow the ideal force generation. Since the criteria that determined the selected set of parameters was to minimise the wing surface, the maximum values allowed for the pitch angle and reduced frequency were selected. The reason is that those parameters increase the performance of the wings without other disadvantage than the possibility of stall (limiting the wing pitch angle) and the power consumption or obtainable maximum frequency (that implies that higher values of the reduced frequency lead to crafting issue).

The task of stabilising the pitch in free flight followed two approaches: aero-

dynamic tail and inertial tail. The fixed aerodynamic tail showed good, reliable results. The open loop control inhibited some improvement, but it has to be taken into account that it requires a heavier tail assembly in order to allow and control the variable deflection. The closed loop control showed to benefit from both a proportional controller and a proportional-derivative controller, but with stability issues in case of insufficient sampling frequency. The closed loop control is the most powerful damping tool by far, since it can be optimised and strengthened as much as desired, being the refreshing rate the limitation due to the instabilities arising on low rates. On the other hand, the inertial tail showed to be powerful enough to damp the oscillations with relatively small deflections, which means that it has margin to operate and manoeuvre in the vertical plane. That manoeuvrability is specially interesting because of the fact that the lack of aerodynamic tail makes the system unstable, but much more manoeuvrable, as opposed to the aerodynamic tail vehicles that are stable but lack of the ability to make quick manoeuvres due to its stable nature.

5.2 Future work

The vehicle design gave priority to simple approaches when decisions had to be made. The purpose was to obtain a vehicle able to fly so that stabilising mechanisms were tested on it, so making it more complex than necessary in order to achieve slight performance gains was not of interest for the development of this project, as would be the case when aiming to design a vehicle to be manufactured. One of the parameters that would need more attention is the reduced frequency, which was too high. It may be reduced to values closer to those expected based on the nature by increasing the wing pitch and flap amplitudes. On top of that and as anticipated on the introduction, higher order methods accounting for viscous effects should be used to obtain more accurate forces.

The aerodynamic tail open loop control can be further refined following the results obtained from the phase shift approach. However, the closed loop controller is the preferred option since it allows adaptation to situations like perturbations such as gusts.

The inertial tail is not thoroughly discussed in this document. Since it is unstable, it is expected to be harder to design a control law able to handle the vehicle without the help of any aerodynamic tail.

With respect to the wing kinematics, including them into the closed loop control is a possibility that was not explored in this document but should be considered in more complex controllers. This has to be dealt carefully since the thrust and lift

depend on that, so modification of the motion laws could cause severe changes on the forces.

It is complicated to try to enumerate all the different improvements that could be done due to the amount of possibilities that flapping wings have to offer. Here are mentioned the options that would make sense to explore after this work, but there are definitely many more.

Appendix A

Tail tabulated coefficients

AoA [deg]	CL [-]	CD [-]	CM_{LE} [-]
-19.5	-0.827267	0.109424	0.17386
-19	-0.808692	0.104407	0.169734
-18.5	-0.789922	0.099469	0.165574
-18	-0.770961	0.094612	0.161382
-17.5	-0.751813	0.089842	0.157158
-17	-0.732482	0.085162	0.152904
-16.5	-0.712972	0.080574	0.148621
-16	-0.693287	0.076084	0.144311
-15.5	-0.673431	0.071694	0.139974
-15	-0.653409	0.067408	0.135613
-14.5	-0.633225	0.063229	0.131228
-14	-0.612883	0.05916	0.126821
-13.5	-0.592389	0.055205	0.122394
-13	-0.571746	0.051366	0.117947
-12.5	-0.55096	0.047647	0.113481
-12	-0.530036	0.044049	0.109
-11.5	-0.508978	0.040577	0.104502
-11	-0.487791	0.037232	0.099991

AoA [deg]	CL [-]	CD [-]	CM_{LE} [-]
-10.5	-0.46648	0.034018	0.095467
-10	-0.445052	0.030936	0.090932
-9.5	-0.42351	0.02799	0.086386
-9	-0.40186	0.02518	0.081833
-8.5	-0.380107	0.02251	0.077272
-8	-0.358257	0.019982	0.072706
-7.5	-0.336316	0.017597	0.068135
-7	-0.314288	0.015357	0.063561
-6.5	-0.292179	0.013265	0.058986
-6	-0.269995	0.01132	0.05441
-5.5	-0.247742	0.009526	0.049836
-5	-0.225424	0.007883	0.045265
-4.5	-0.203048	0.006393	0.040697
-4	-0.18062	0.005057	0.036135
-3.5	-0.158145	0.003875	0.03158
-3	-0.135629	0.00285	0.027033
-2.5	-0.113078	0.00198	0.022495
-2	-0.090498	0.001268	0.017969
-1.5	-0.067894	0.000714	0.013455
-1	-0.045272	0.000317	0.008954
-0.5	-0.022639	0.000079	0.004469
0	0	0	0
0.5	0.022639	0.000079	-0.004451
1	0.045272	0.000317	-0.008883
1.5	0.067894	0.000714	-0.013294
2	0.090498	0.001268	-0.017684
2.5	0.113078	0.00198	-0.02205
3	0.135629	0.00285	-0.026392
3.5	0.158145	0.003875	-0.030708
4	0.18062	0.005057	-0.034997
4.5	0.203048	0.006393	-0.039257
5	0.225424	0.007883	-0.043487

AoA [deg]	CL [-]	CD [-]	CM_{LE} [-]
.5	0.247742	0.009526	-0.047687
6	0.269995	0.01132	-0.051854
6.5	0.292179	0.013265	-0.055987
7	0.314288	0.015357	-0.060086
7.5	0.336316	0.017597	-0.064148
8	0.358257	0.019982	-0.068173
8.5	0.380107	0.02251	-0.07216
9	0.40186	0.02518	-0.076106
9.5	0.42351	0.02799	-0.080012
10	0.445052	0.030936	-0.083876
10.5	0.46648	0.034018	-0.087696
11	0.487791	0.037232	-0.091471
11.5	0.508978	0.040577	-0.095201
12	0.530036	0.044049	-0.098885
12.5	0.55096	0.047647	-0.10252
13	0.571746	0.051366	-0.106106
13.5	0.592389	0.055205	-0.109642
14	0.612883	0.05916	-0.113127
14.5	0.633225	0.063229	-0.116559
15	0.653409	0.067408	-0.119938
15.5	0.673431	0.071694	-0.123263
16	0.693287	0.076084	-0.126532
16.5	0.712972	0.080574	-0.129746
17	0.732482	0.085162	-0.132901
17.5	0.751813	0.089842	-0.135999
18	0.770961	0.094612	-0.139037
18.5	0.789922	0.099469	-0.142015
19	0.808692	0.104407	-0.144932
19.5	0.827267	0.109424	-0.147787
20	0.845644	0.114516	-0.150579

Table A.1: Tail coefficients

Appendix B

Project budget

In this section are described the different items that contribute to the project budget.

MATLAB license. All the computations in this project were performed with Matlab. Individual academic licenses cost 500€.

Personal Computer. The computer used to code and process the results, as well as writing the document, includes a Intel-i5 processor and it is priced at €800. The screen used for display costed €100. The total hardware cost is €900.

Computational time Since simulations are time consuming (even in this low order approach) and parametric studies have been conveyed, a High Performing Computer Cluster has been used to perform the simulations. Spanish CESGA centre offers their clusters at an average price of €0.15 per CPU per hour. This project required CPU hours are estimated to be 800h at 2 CPU. Therefore, the total computational cost is €240.

Worker salary The price per work hour for a recent graduate in the post-crisis Spain can be estimated at 7€. Since the time required for this project has been 700h, the total cost of of the personnel is €4,700

The sum of the elements listed above makes a total budget of €6340.

Bibliography

[1] Pesavento, Umberto, and Z. Jane Wang. 'Flapping wing flight can save aerodynamic power compared to steady flight.'Physical review letters 103.11 (2009): 118102.

[2] Mueller, Thomas J. Fixed and flapping wing aerodynamics for micro air vehicle applications. Vol. 195. AIAA, 2001.

[3] Shyy, Wei, et al. An introduction to flapping wing aerodynamics. Vol. 37. Cambridge University Press, 2013.

[4] Fry, Steven N., Rosalyn Sayaman, and Michael H. Dickinson. 'The aerodynamics of free-flight maneuvers in Drosophila.'Science 300.5618 (2003): 495-498.

[5] Marey, E. J. 'Determination experimentale du mouvement des ailes des insectes pendant le vol.'CR Acad. Sci. Paris 67 (1868): 1341-45.

[6] Wang, Z. Jane. 'Dissecting insect flight.'Annu. Rev. Fluid Mech. 37 (2005): 183-210.

[7] Jensen, Martin. 'Biology and physics of locust flight. III. The aerodynamics of locust flight.'Philosophical Transactions of the Royal Society of London B: Biological Sciences 239.667 (1956): 511-552.

[8] Grauer, Jared, et al. 'Testing and system identification of an ornithopter in longitudinal flight.'Journal of Aircraft 48.2 (2011): 660-667.

[9] De Croon, G. C. H. E., et al. 'Design, aerodynamics, and vision-based control of the DelFly.'International Journal of Micro Air Vehicles 1.2 (2009): 71-97.

[10] De Wagter, Christophe, et al. 'Autonomous flight of a 20-gram flapping wing mav with a 4-gram onboard stereo vision system.'Robotics and Automation (ICRA), 2014 IEEE International Conference on. IEEE, 2014.

[11] EU Commission. "Communication from the commission to the European parliament and the council: A new era for aviation—opening the aviation market to the civil use of remotely piloted aircraft systems in a safe and sustainable manner." (2014).

[12] SESAR. "Small RPAS Operations Near Regional Airports." (2015)

[13] Latvian Presidency of the Council of the European Union. "Framing the future of aviation." (2015)

[14] Pennycuick, C. 'Wingbeat frequency of birds in steady cruising flight: new data and improved predictions.'Journal of Experimental Biology 199.7 (1996): 1613-1618.

[15] Arranz, G. 'DEVELOPMENT OF AN UNSTEADY POTENTIAL MODEL FOR A FLAPPING WING MAV.'Universidad Carlos III de Madrid (2015)

[16] Katz, Joseph, and Allen Plotkin. Low-speed aerodynamics. Vol. 13. Cambridge University Press, 2001.

[17] Martínez, B. 'Dynamic models for Flapping-Wing Micro-Air Vehicles'Universidad Carlos III de Madrid (2015)

[18] Tewari, Ashish. Atmospheric and space flight dynamics. Birkhuser Boston, 2007.

[19] Muijres, F. T., et al. "Leading-edge vortex improves lift in slow-flying bats." Science 319.5867 (2008): 1250-1253.

[20] Birch, James M., and Michael H. Dickinson. "Spanwise flow and the attachment of the leading-edge vortex on insect wings." Nature 412.6848 (2001): 729-733.

[21] Triantafyllou, M. S., G. S. Triantafyllou, and D. K. P. Yue. "Hydrodynamics of fishlike swimming." Annual review of fluid mechanics 32.1 (2000): 33-53.

[22] Tipler, Paul A., and Gene Mosca. Physics for scientists and engineers. Macmillan, 2007.

[23] Etkin, Bernard, and Lloyd Duff Reid. Dynamics of flight: stability and control. Vol. 3. New York: Wiley, 1996.

[24] Anderson Jr, John David. Fundamentals of aerodynamics. Tata McGraw-Hill Education, 1985.

[25] Ogata, Katsuhiko. Modern control engineering. Prentice Hall PTR, 2001.